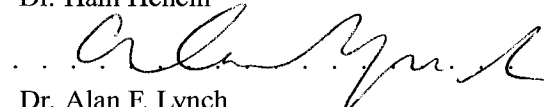**University of Alberta**

**Faculty of Graduate Studies and Research**

The undersigned certify that they have read, and recommend to the Faculty of Graduate Studies and Research for acceptance, a thesis entitled **Hot Strip Finishing Mill Modeling and Looper Control** submitted by Sansal K Yildiz in partial fulfillment of the requirements for the degree of **Master of Science** in *Process Control*.

Dr. J. Fraser Forbes (Supervisor)

Dr. Biao Huang (Co-Supervisor)

Dr. Hani Henein

Dr. Alan F. Lynch

Date: 3rd of August 2005

**University of Alberta**


HOT STRIP FINISHING MILL MODELING AND LOOPER CONTROL


by


**Sansal K Yildiz**

©


A thesis submitted to the Faculty of Graduate Studies and Research in partial fulfillment of the requirements for the degree of **Master of Science**


in


Process Control


Department of Chemical and Materials Engineering


Edmonton, Alberta
Fall 2005

**Canada**

<div align="center">

**University of Alberta**

**Library Release Form**

</div>

**Name of Author**: Sansal K Yildiz

**Title of Thesis**: Hot Strip Finishing Mill Modeling and Looper Control

**Degree**: Master of Science

**Year this Degree Granted**: 2005

Permission is hereby granted to the University of Alberta Library to reproduce single copies of this thesis and to lend or sell such copies for private, scholarly or scientific research purposes only.

The author reserves all other publication and other rights in association with the copyright in the thesis, and except as hereinbefore provided, neither the thesis nor any substantial portion thereof may be printed or otherwise reproduced in any material form whatever without the author's prior written permission.

Sansal K Yildiz

Date: 10th of August 2005

# Abstract

Finishing mill control is vital in meeting the product dimensional quality requirements for hot sheet rolling. In a finishing mill, strip tension is regulated by loopers to ensure a uniform strip width. Various modern control approaches have been applied so far to improve looper control, including: optimal, inverse linear quadratic, H-infinity and robust control. In this study, a computer simulation of a finishing mill has been developed to design and evaluate new control strategies. The model has been validated against real plant data and can predict the looper motion and phenomena such as deformation, heat transfer and slip. It is nonlinear and accounts for the variable inter-stand transport delay. Looper covariance controllers have been designed and tested using the simulator. It has been found that covariance control provides a more stable operation compared to the conventional control, and use of speed disturbance information in feedforward mode significantly enhances any form of looper control.

# Acknowledgements

My first thanks go to my supervisor Dr Fraser Forbes and Dofasco's Mike Dudzic for coming up with the nice idea of starting this project and making the necessary and quite troublesome arrangements for my visit to Dofasco. I had many fruitful discussions with my co-supervisor Dr Biao Huang, who was eager to meet me whenever I had concerns regarding the control theory or practice. Dr Yale Zhang of Dofasco also deserves special thanks here for making everything so smooth during my two weeks stay in Hamilton and for his committed support to this project. I finally wish to thank all of the Dofasco personnel who contributed to my understanding of the practical issues of hot strip mill operation, and especially to Fred Wang, whose expertise in looper control and patience to answer my quite subtle questions proved to be very valuable.

*"Megalomania is the only form of sanity."*

\- Churchill

# Contents

# List of Tables

# List of Figures

# List of Symbols

| | |
|---|---|
| $a$ | lever factor |
| $\alpha_r$ | roll thermal diffusivity |
| $b_1 - b_3$ | calibration coefficients for thermal equations |
| $C$ | roll gap under no load |
| $c_f$ | looper viscous damping coefficient |
| $c$ | strip specific heat capacity |
| $\Delta T_c$ | strip temperature drop due to conduction |
| $\Delta T_m$ | strip temperature gain due to deformation work |
| $E$ | strip modulus of elasticity |
| $E_r$ | roll modulus of elasticity |
| $\epsilon$ | strip surface emissivity |
| $\dot{\epsilon}$ | mean strain rate |
| $F$ | deformation force |
| $f$ | forward slip factor |
| $G_r$ | gear ratio |
| $h$ | strip gage |
| $J$ | total inertia on looper motor |
| $J_0$ | machine inertia on looper motor |
| $J_c$ | total inertia on coiler motor |
| $J_{c0}$ | machine inertia on coiler motor |
| $J_{md}$ | main drive inertia on motor |
| $K$ | deformation resistance |
| $K_c$ | main drive PI speed regulator gain |
| $K_s$ | stand stiffness |
| $k$ | strip oxide layer thermal conductivity |
| $L$ | inter-stand strip length |
| $L_0$ | inter-stand strip length under no tension |
| $M$ | looper motor torque output |
| $M_c$ | coiler motor torque output |
| $M_D$ | main drive torque output |
| $M_F$ | total dissipative load on looper |
| $M_L$ | total looper load |
| $M_R$ | total roll torque |

| | |
|---|---|
| $m_L$ | looper mass |
| $\mu$ | roll-strip friction coefficient |
| $\nu_r$ | Poisson's ratio for roll material |
| $\omega$ | work roll angular speed |
| $\omega_c$ | coiler motor angular speed |
| $\omega_L$ | looper angular speed |
| $Q$ | deformation geometry factor |
| $R_0$ | work roll radius under no load |
| $R$ | deformed work roll radius |
| $R_c$ | coiler mandrel radius |
| $r$ | reduction |
| $r_c$ | coil radius |
| $r_L$ | looper center of gravity radius |
| $\rho$ | strip density |
| $S$ | Stefan-Boltzmann constant |
| $s_f$ | static looper friction load |
| $\sigma$ | strip tension |
| $\bar{\sigma}$ | strip mean shear yield stress |
| $\sigma_y$ | strip tensile yield stress |
| $T$ | strip temperature |
| $T_r$ | effective work roll temperature |
| $\tau$ | transport delay |
| $\tau_{cr}$ | looper current regulator time constant |
| $\tau_I$ | main drive PI speed regulator reset time |
| $\tau_{pr_{1,2}}$ | roll position regulator time constants |
| $\theta$ | looper angle |
| $V_c$ | strip entry speed to coil |
| $v$ | strip speed |
| $w$ | strip width |
| $z_a$ | arithmetic average aspect ratio |

*"He has many good qualities, some of which lie hidden, and he has many*
*bad qualities, all of which are in the shop window."*
— Field Marshal Sir H Wilson on Churchill

# 1

# Introduction

This chapter defines the objective and scope of the thesis and lays the background necessary for understanding the issues of finishing mill modeling and control. In this context, the hot strip mill, in particular the finishing train, its operation, its control objectives and main disturbances, and finishing mill control strategies adopted thus far are introduced. Being closely related to control, finishing mill modeling is also briefly examined.

## 1.1  Thesis Objective and Scope

Hot rolling is an essential industrial process which produces sheet steel, a widely used product in manufacturing and construction. Hot mills are primary assets with millions of tons of annual output and billions of dollars of revenues, and their optimal and continuous operation has to be maintained to survive in today's very competitive steel market. The customer demand on the dimensional quality of the rolled steel has also increased in past two decades. These facts make modern control a vital part of the rolling process, especially of the finishing mill, which is the high-tech final part of a hot mill.

In a finishing mill, inter-stand strip tension is regulated by strip storage devices called loopers. Minimization of tension fluctuations ensures a more uniform strip width and thus

1

contributes to a reduced operating cost. Tension control can be improved by installing better quality looper equipment and also by using advanced control techniques. Looper control, which is traditionally multi-loop, has been the subject of considerable industrial and academic interest in past two decades and various multivariable feedback control theories such as optimal, inverse linear quadratic, H-infinity and robust control have been applied. Most of these systems have been reported to be in successful commercial operation.

Although the looper controllers of a finishing mill typically work independently of each other, it is important to understand the dynamics of the whole mill adequately before attempting the controller design. The finishing mill is a complex plant with strong interactions between its units and local changes might have unexpected plant-wide consequences. Thus, a detailed, high fidelity hot strip mill model becomes a very important asset for control design. Such a model will enhance the understanding of the overall plant behavior as well as constituting a basis for control performance evaluation.

It is the first objective of this study to develop a finishing mill simulator and validate it against real plant data. In modeling of a complex plant such as a finishing mill, proper choice of the phenomena to be modeled is very important and will be made considering the end use of the model. Since the model is intended for controller design and testing, issues such as variable transport delays, dynamics of the plant actuators and proper modeling of disturbances should be given priority. On the other hand, models for phenomena such as deformation and heat transfer, which indirectly affect looper control, do not need to produce very accurate numerical results as long as they represent the physics of the phenomena adequately. For most of the phenomena taking place in a finishing mill there are models or relationships available in literature. Thus, carrying out a detailed literature survey will be the first task.

Application of the covariance control theory to the looper control problem is the second objective of this study. A covariance controller is a combined observer-state feedback system that minimizes the control energy, while ensuring that the design constraints on the controlled variables' covariances are not violated. The linear model required for multivariable controller design will be obtained from the finishing mill simulator, which

will also serve as a means of performance assessment. In order to obtain a benchmark controller to which the covariance controllers can be compared, a conventional control system will be designed. Finally, the benefits of a speed feedforward loop that is commonly employed in finishing mills will be evaluated.

## 1.2 Hot Strip Mill

A hot strip mill rolls cast steel slabs into thin sheets. A typical hot strip mill facility consists of, in written order, the following units: Reheat furnace, roughing mill, transfer table, coilbox, crop shear, finishing mill, runout table and coiler. A layout is given in Figure 1.1.
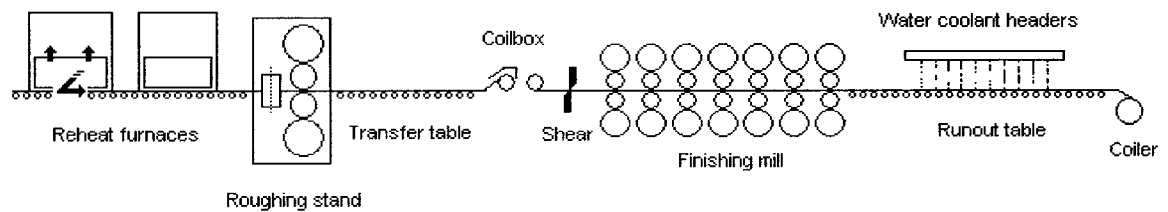


Figure 1.1: Layout of a semi-continuous hot strip mill with 1 reversing rougher

The reheat furnace ensures that the slab is at a suitable temperature to start hot rolling, which is approximately 1200°C. The next unit, the roughing mill, is responsible for major reductions in slab thickness (e.g. a reduction from 200 mm to 30 mm) and width. The slab could be as much as 9 m long and in the rougher its length increases proportionally with the reduction since the width remains almost constant. The rougher may have one or more stands, thus specifying the level of continuity of the facility. In all arrangements except fully continuous, one stand is reversing, meaning that the slab is rolled back and forth until it is reduced to the desired thickness before proceeding to continuous rolling. A fully continuous mill has four or more roughing stands. The transfer (delay) table carries the transfer bar from the roughing mill to the finishing mill. The transfer bar is typically 40-80 m long and 0.5-1.5 m wide. A relatively recent development in hot strip mill design, the coilbox, is sometimes used to reduce the temperature drop between the head and tail ends of the strip. In this type of application the transfer bar is coiled in the coilbox after the roughing mill and then peeled to be fed to the finishing mill. The coilbox significantly

reduces the heat losses and can bring the total temperature drop down to 10°C from the usual value of around 100°C without a coilbox. In hot strip mills there are scale-breakers also, usually located before the roughing mill and the finishing mill. They wash the scale (iron oxides) away using high speed jets of water or steam, sometimes after mechanically loosening it [9, 27].

## 1.3 Finishing Mill

A 7-stand finishing mill is shown in Figure 1.2 together with the runout table and coiler. Typical values for strip thickness, temperature and speed are also given. A 4-high mill stand consists of two work rolls and two backup rolls supporting them, the former having a smaller diameter as seen in Figure 1.2. The backup roll supports the work roll to mitigate the deflection caused by the deformation force. A typical work roll has a diameter of 750 mm and the backup roll has twice thereof. Each stand has its own drive unit, the main drive, to power the work rolls. The main drive may include a single motor driving both rolls simultaneously through a gear box or two motors each driving one roll [9]. The distance between the work rolls, or briefly the roll gap, is adjusted by positioning the backup rolls. The positioning is achieved either by conventional electric screws or more recent and faster hydraulic actuators. These are generally installed above top backup roll chucks or under bottom backup roll chucks[9]. To alleviate the strip flatness problems caused by roll deflection, a roll bending system may be installed on some stands. It consists of hydraulic jacks that force the roll chucks in the opposite direction of deflection and may operate on the work roll or backup roll chucks only, or both [9]. Rolls with curved designs are also used and laterally shifted during rolling to overcome the deflection problems.

Between the stands are the loopers, the strip storage units shown in Figure 1.2. A looper is a metal cylinder supported by an arm free to move around a pivot. It may be driven by an electric motor, or by hydraulic or pneumatic means. Keeping the strip above the pass line, it stores the extra amount of strip that is necessary for strip tension regulation. A speed mismatch between adjacent stands causes a tension change, upon which the looper moves and tries to compensate. The looper function is not unlimited and can require the intervention of the drive speed regulators, as any permanent speed mismatch will
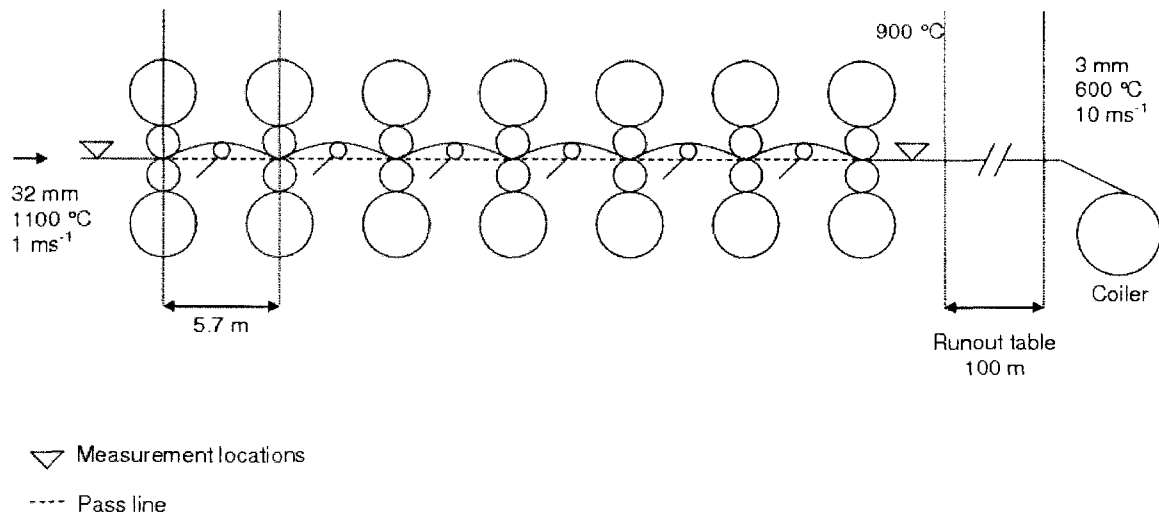
Figure 1.2: Layout of a 7-stand finishing mill

inevitably consume the stored strip or increase the loop length beyond the looper's reach. Proper tension regulation is essential for safe operation and good strip width performance. Nominal tension values increase from around 5 MPa after the first stand to 10 MPa or so before the last.

The strip emerging from the finishing mill is typically much longer than the runout table; so, the coiling starts before the tail end leaves the finishing mill. The strip is cooled by the water from coolant headers along the runout table. When the strip is released from the last stand, pinch rolls near the coiler squeeze the strip in order to maintain the coiler tension, which is generally around 5 MPa.

Because of the extreme environment and a lack of space in the finishing mill, it is not easy to install and maintain sensors. Consequently, few measurements are available. The common practice is to measure the strip temperature at the inlet; and temperature, profile and shape at the exit. Temperature is measured by pyrometers and profile by an X-ray gage. Width may also be measured. There are generally no direct measurements of the strip properties along the finishing mill. Looper positions and backup roll forces are typically the only measurements from which the gage (thickness) and tension are inferred. Strip tension and looper speed may sometimes be measured, the former via a load cell placed on the looper roll.

# 1.4 Finishing Mill Control Objectives

Uniform strip dimensions, desirable strip delivery temperature and safe operation are the ultimate objectives. Finishing mill control is mainly a regulation problem. Each stand's controller regulates the control variables around the setup values specified before the operation.

Gage, width, profile and shape are the main dimensional indicators. Gage here may be understood as the strip centerline thickness. Profile is a sectional view across the width of the strip and has therefore to do with cross sectional thickness variations. Due to roll deflection, a strip is typically thicker in the center, a profile known as crown. A slight crown is necessary to track the strip [30] but otherwise it should be kept within the tolerances. Mismatch of the incoming strip and deflected roll profiles leads to different amounts of elongation across the width and, consequently, to stored stresses. These stresses, if excessive, will cause shape (flatness) problems, which may be in form of wavy edges or buckles, or may not be manifest unless the strip is slitted[9].

Gage is controlled via regulation of the roll gap. In a finishing mill there is no actuator directly affecting the width but proper regulation of other dimensional properties and the strip tension ensures uniform width. High strip tension may cause the strip to shrink in width [25]. Roll bending systems control the profile by changing the amount of roll deflection. As the shape and profile are interactive, manipulations of the profile should be constrained lest the shape is affected beyond limits. The delivery temperature is controlled to ensure the desired metallurgical properties. Especially, it should not be allowed to drop below the austenization temperature because this would lead to a sudden decrease in the deformation force. Interstand cooling rates and rolling speed are manipulated to control the delivery temperature.

In addition to causing poor product quality, inadequate tension control may lead to instability and cobbling and may eventually damage the rolls and cause downtime. Hence it has ramifications on both plant safety and economics.

# 1.5 Finishing Mill Disturbances

Nonuniform strip properties and mill structural imperfections such as eccentric rolls are the main disturbances in a finishing mill which adversely affect both strip dimensional accuracy and looper control. These disturbances usually have very specific frequency and magnitude ranges and knowledge of these ranges is essential to determine the control bandwidth.

In a hot strip mill each stand has its own controllers; thus, it is necessary to investigate the disturbances on a stand basis, rather than considering the mill as a whole. The following disturbances are transmitted to the stands by the strip:

1. Entry temperature,

2. Entry gage,

3. Entry speed to downstream stand,

4. Entry tension.

Strip entry temperature naturally decreases in time because the tail end of the strip experiences a longer period of radiative heat loss. If no coilbox is used, this drop could be around 100 °C in total. The temperature disturbance has also a cyclic nature due to skid marks, the cold regions caused by the bars that hold the slab in the reheat furnace. Entry gage is simply the delayed gage from the previous stand. To regulate the exit gage, stand gage controller acts according to the force changes caused by entry temperature and gage, thus disturbing the strip speed on both sides of the stand. This is the main cause of the speed fluctuations which disturb the upstream stand. For the downstream stand it manifests itself as an entry tension fluctuation, which is less of a disturbance compared to speed changes.

Roll eccentricity is a general term implying the out-of-roundness of backup or work rolls, or a misalignment of the bearings and the roll body [9]. Disturbing the roll gap, it causes gage deviations and eventually contributes to strip speed changes. Since roll rotation speeds are precisely known, eccentricity effects can easily be detected in spectral analysis of the plant data. Due to high frequency of rotation, even a slight eccentricity may significantly disturb the looper system. When the misalignment reaches a critical size, the roll is replaced.

In a hot strip mill there are various control systems other than the looper controllers. In gage and profile control for example, multiple loops may exist. As far as looper control design is concerned, the effects of such loops should also be considered disturbances because in practice most of them operate independently of the looper controller.

# 1.6 Tension and Gage Control

Loopers and roll position actuators are used to control the tension and gage. The looper, however, should remain within a certain position range or it may become unstable under linear controllers. The objectives of thickness and looper control are, then:

1. Regulating the interstand tension,

2. Constraining the looper position,

3. Regulating the gage.

Gage controller may cooperate with profile controller and with some other control loops. This sort of advanced profile control arrangements are beyond the scope of this study.

Gage control is a disturbance to tension due to the strip speed fluctuations it causes. Tension fluctuations in turn disturb the thickness, although not as strongly. Despite these interactions, the conventional approach is to keep gage and tension regulators independent. While it works well with electric screws as roll actuators, it is less robust when much faster hydraulic actuators are used.

Considering the interactive nature of the finishing mill control objectives, various multivariable controllers have been designed, each replacing some independent loops of the conventional systems.

## 1.6.1 Conventional control

At this basic level of finishing mill control, thickness is controlled by a system named AGC (Automatic Gage Control) and looper angle is controlled by a PI regulator that works with looper angle feedback and trims the upstream main drive speed. The looper motor torque

is manipulated to regulate the strip tension. Thus, there are three independent loops, all shown in Figure 1.3.
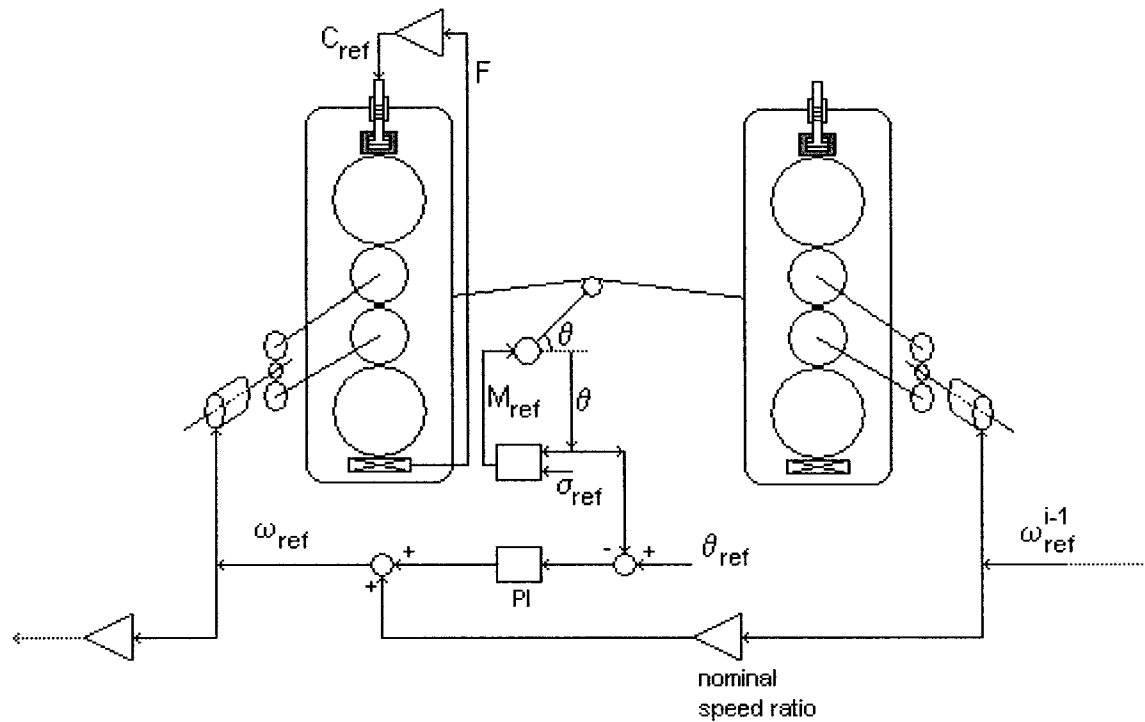


Figure 1.3: Conventional looper and gage control arrangement

AGC, as modeled here, is a proportional controller inferring the changes in stand deflection from the force measurements and readjusting the gap accordingly. The looper torque controller is a static, nonlinear feedback loop calculating the necessary torque to obtain the reference strip tension at any given looper angle.

The speed reference signal from the downstream stand is notable here. As what really matters is the relative speeds of the adjacent stands, rather than the absolute speed of a single stand, this signal is vital. It may be considered a feedforward signal since, being a reference signal, it helps in estimating what the downstream strip entry speed in the next moment will be, rather than the current strip speed.

## 1.6.2 Multivariable tension control

Recognizing the interaction between the looper position and strip tension, various multivariable controllers have been designed combining the position and tension control loops. Examples are the H-infinity controller [17], inverse linear quadratic (ILQ) controller [18] and optimal multivariable controller [29]. It is reported that these controllers have been commissioned in commercial operation with better performance.

Instead of the looper motor torque (motor current) used in conventional control, looper angular speed is chosen as the manipulated variable in all these designs. Seki *et al.* [29] state that the speed control loop can better absorb the changes in looper load compared to the current control loop. This is not surprising, given that the speed regulator uses looper speed feedback, which is typically not used in current control arrangements.

## 1.6.3 Multivariable tension and gage control

If tension and gage control loops are combined in a single multivariable controller, the strip speed disturbances caused by the thickness control action can be better tolerated. This is exactly the idea behind Hearns and Grimble's multivariable [14] and later, robust multivariable [15] controllers. An improved version of the speed feedforward loop described in §1.6.1 is also present here. Instead of the downstream stand speed, an estimation of the strip entry speed to the downstream stand is used as a feedforward variable. Estimation is made using a model and some information from the downstream stand. Other disturbances are considered as filtered white noise. The H-infinity control theory is employed.

Okada *et al.* [22] first treat the mill as a whole and then find that the stands can be decoupled and controlled independently if a similarity transformation is used. It should be noted, however, that the model leading to this conclusion is discrete and approximates the transport delays using the sampling increments. Transport delay actually depends on mill speed, which is generally increased throughout the operation. The controller for each stand is then designed based on optimal servo control theory. This system has been reported to be in successful commercial operation.

Looper torque, not the speed, is used as the manipulated variable in both designs. It

appears that the later design has strip tension and thickness measurements available at each stand, since these are used as feedback, but no mention of an estimator is made.

A slight modification to the approach outlined above has been made by Hearns *et al.* [16]. Based on the fact that the strip tension is a relatively small disturbance to thickness and the conventional tension control has good performance provided that the looper position is controlled well, the tension control is not included in this design. In other words, the thickness and looper position control loops of the conventional method are combined under a multivariable controller but the nonlinear, static tension regulator is retained. A test trial of this system between stands 4 and 5 of a 7-stand finishing train has shown a small improvement over conventional control.

### 1.6.4 Use of speed feedforward in tension and gage control

In addition to the aforementioned methods, there is a quite interesting feedforward approach, mostly demonstrated by Austrian researchers Rigler *et al.* [26] and Keintzel *et al.* [19], and also briefly mentioned by Stephens *et al.* [32] and Bilkhu *et al.* [1].

This system heavily rests on a Kalman filter predicting the thickness and temperature along the mill and a buffer system that has to segment and track the strip rather precisely. The Kalman filter has the measured force and stand speed as inputs. The tracking algorithm is based on a slip model, which uses stand speed, strip thickness and tension. As stated by both authors, care has to be taken to remove the strip tracking errors, given that feedforward action is used. The system is in commercial operation.

Knowledge of strip gage and temperature at any point and time along the mill is a major asset for control. Such knowledge can be easily utilized in two ways:

1. For tension control, as the upstream stand's speed can be better controlled when the strip entry speed to the downstream stand is estimated, which can be readily made using the information from the strip tracking system.

2. For thickness control, as the roll can be adjusted right on time when the incoming thickness disturbance is predicted.

Proper handling of the transport delay is the distinct advantage of this approach. Even

a linear, multivariable system controlling the whole plant cannot emulate this; since, in a linear design, the transport delay has to be somehow approximated and its variation in time can not be accounted for by conventional control approaches.

## 1.7 An Overview of Supervisory Profile and Shape Control

Local regulation of strip tension may be sufficient for the purposes of hot rolling; however, profile and shape control could be improved by a supervisory (coordinating) controller that manipulates certain regulator setpoints.

The need to change the setpoints is a result of the setup errors. As explained in Section 1.4, the profile cannot be arbitrarily controlled because the shape may be adversely affected. The total thickness reduction and profile change should therefore be distributed among the stands in a way that the shape does not deteriorate beyond limits. Redistribution of the amounts of per stand reduction and profile changes based on the measured output errors and input constraints constitutes the task of the supervisory controller here.

Model predictive control (MPC) is one suitable choice, especially considering the input constraints. Such a controller has been studied by Bulut et al., who considered the last three stands of a 7-stand finishing mill [2]. In this study, using the roll bending moment and the roll gap as constrained inputs, thickness and shape are controlled. Grimble et al. designed a similar predictive optimal controller to supervise the thickness and profile setpoints [10]. Both designs employ a rather simplified model and appear to be more of simple feasibility studies.

## 1.8 Modeling of the Finishing Mill

From a practical point of view the phenomena of interest in a finishing mill fall into two:

1. Those for which a dynamic model is necessary and available,

2. Those which can (or have to) be approximated with constitutive relationships.

The motion of the looper and other actuators are in the first category; deformation, temperature and slip models generally in the second. The second category has often fast enough dynamics to justify the approximation. Thus, the finishing mill model is a set of differential and algebraic equations (DAE's) that must be simultaneously solved.

Another important phenomenon, the interstand transport delay, may be handled in a variety of ways. As far as the mathematical description is considered, in a continuous time model it has to be somehow approximated; in a discrete model approximation is inherent. It is variable, however, and is properly handled via mechanisms such as simulation software that allow buffers.

### 1.8.1 The dynamic relationships

Models describing looper and tension dynamics are abundant in literature, especially the hot strip mill control literature, and are essentially the same. The often quoted work of Price [25] is perhaps one of the earliest and gives a simplified geometric analysis of the strip-looper system, and a linear model. A nonlinear model that appears in many of the articles written by Hearns and Grimble [14, 15] is one of the most comprehensive models available in the literature. The relevant parts of the linear models often used in controller design can be obtained by linearizing this model. Unfortunately, the numeric values of the constants are usually not given.

In control related work, the actuators such as the roll positioning system, main drive or looper current regulator are generally simplified as first order lags. For simulation models, a more rigorous approach should be preferable. In his cold mill modeling work, Guo [12] simply uses a second order lag element for both the screws and hydraulic roll actuators but treats the main drive more carefully, taking into account the system inertia and the roll torque disturbance. Detailed mill drive models accounting for the inertia and stiffness of the parts, friction, and controller dynamics are available in literature [5, 33]. Guo [11]himself models a hydraulic roll actuator rather rigorously.

## 1.8.2 The constitutive relationships

Prediction of the deformation force is no straightforward task, even when the workpiece temperature, the most influential variable whose prediction is another difficult task, is accurately known. Although there are numerous methods to predict the roll force and they agree in a qualitative sense, there are substantial differences in quantity. Most of the available methods have been derived from the earlier work of Orowan with various simplifications and all have empirical parts. One solution is to use the analytical part of one of these methods, especially that of Sims, and replace the empirical part with a new one minimizing the prediction error [23, 28, 35].

Along the finishing train, the strip transfers heat in various forms. Due to a lack of measurements, individual contributions of these are not precisely known, which often leads to substantially different estimates of the heat transfer coefficients. Moreover, due to roll cooling and three dimensional nature of the heat transfer, it is difficult to estimate the roll surface temperature, which is required to calculate the conduction loss. The roll surface temperature is generally estimated using a two dimensional heat transfer equation [23, 31]. Heat transfer coefficients have to be estimated based on the available data.

There are numerous equations to calculate the amount of slip between strip and roll. These equations differ as to which variables should be taken into account. Examples are [6, 7, 20, 21, 26].

# 2

# Modeling of the Finishing Mill

The model developed here is intended to test the controller performance. It will also be used for controller design after being linearized and simplified as necessary. As the main objective is to improve the tension control, profile and shape are not considered and the strip is modeled as an elastic string. The emphasis is naturally given to the model's dynamic and qualitative features, rather than the numerical accuracy of its predictions. A model that can accurately describe the phenomena such as plastic deformation, heat transfer and slip over a whole range of operating points and products would be beyond the scope of this project.

There is not a wealth of information regarding the finishing mill simulations in the literature. One of the highest fidelity models has been developed in a joint project by Kvaerner Metals, British Steel, Alcan, Cegelec and the Industrial Control Center of the University of Strathclyde for a 5-stand finishing mill [3]. It is nonlinear and includes profile and shape. No details of this model is given. A simpler model that does not include profile and shape is presented in some detail by Rigler et al. [26]. A high degree of accuracy has been reported for both models. Other models that have been found in the literature are not intended for simulations but rather are partial, simplified and linearized sets of equations useful for controller design. Numerical values for model constants are typically not provided.

15

## 2.1  Simplified Plant

A schematic drawing of the simplified basic mill unit to be modeled is shown in Figure 2.1. The inlet variables to the stand are designated by upper-case letters and the exit variables are designated by lower-case letters. A nomenclature list can be found at the beginning of



Figure 2.1: A schematic drawing of the stands, looper and the strip

the thesis clarifying some of the variables used in Figure 2.1 and defining the variables that will be used in the following sections.

## 2.2  Looper-Strip System

Strip tension between stands $i$ and $i + 1$ can be expressed using Hooke's law:

$$\sigma = \Sigma_{i+1} = E\frac{L - L_0}{L_0} \tag{2.1}$$

The strip length $L$ is purely a geometric quantity and depends on the looper angle $\theta$ only. From Figure 2.1:

$$L = L_L + L_R \tag{2.2}$$

$$L_L = [(d + l\cos\theta)^2 + (l\sin\theta + r_l - y)^2]^{1/2} \tag{2.3}$$

$$L_R = [(D - d - l\cos\theta)^2 + (l\sin\theta + r_l - y)^2]^{1/2} \tag{2.4}$$

The strip length under no tension $L_0$ is simply the amount of tension-free strip stored between the stands. Its rate of change is:

$$\frac{dL_0}{dt} = \frac{v - V_{i+1}}{1 + \sigma/E} \tag{2.5}$$

Differentiating Equation 2.1 and combining with Equation 2.5:

$$\dot{\sigma} = \frac{E(1 + \sigma/E)}{L}(\dot{L} - v + V_{i+1}) \simeq \frac{E}{L}(\dot{L} - v + V_{i+1}) \tag{2.6}$$

The approximation above is fairly safe for a finishing mill where the strip tension $\sigma$ is typically 4 or 5 orders of magnitude smaller than the elastic modulus $E$. As stated before, $L$ only depends on the looper angle $\theta$. So:

$$\dot{L} = \frac{dL}{d\theta}\frac{d\theta}{dt} = \frac{dL}{d\theta}\dot{\theta} \tag{2.7}$$

and Equation 2.6 becomes:

$$\dot{\sigma} = \frac{E}{L}\left(\frac{dL}{d\theta}\dot{\theta} - v + V_{i+1}\right) \tag{2.8}$$

Newton's law of motion can be written for the looper:

$$J\ddot{\theta} = M - M_L - c_f\dot{\theta} - s_f\text{sign}(\dot{\theta}) \tag{2.9}$$

Here, $J$ is the total inertia of the looper, looper drive and the strip on looper motor. Strip inertia is significant especially for the earlier stands where the strip is heavier. Its effect may be approximated in the form of a contribution to looper and drive inertia $J_0$ if a linearized and simplified model is used. For practical looper angles, the total inertia on looper shaft $J$ may be approximated as (Appendix A):

$$J = J_0 + \frac{1}{30}D^2hw\rho l\cos\theta \tag{2.10}$$

where the second term is the strip's inertial contribution. It is found that the second term amounts to less than 10% for the strip with a cross sectional area of 7000 mm² or smaller, which is often the case for Loopers 4 to 6.

Damping of the looper-strip system may be ascribed to looper friction, energy dissipated by the strip and vibration of the masses connected thereto. Looper friction should have a threshold value and it also possibly increases with increasing vertical load on the looper. This static friction may be approximated by the constant term $s_f$ in Equation 2.9, neglecting the effect of the force variation. It is common practice to model the damping as viscous friction with a lumped coefficient [15, 26], like the $c_f$ term of Equation 2.9.

The load torque $M_L$ on the looper is caused by the strip tension, strip weight, looper's own weight and the force required to bend the strip. The bending moment is negligible for thin strip but could be of some importance for the first and second loopers of a finishing train where the strip may not be very thin. Using the nomenclature in Figure 2.1, the torque due to the strip tension $M_\sigma$ is:

$$M_\sigma = \sigma w \bar{h} [(- \cos \alpha_L + \cos \alpha_R)(l \sin \theta + r_l) + (\sin \alpha_L + \sin \alpha_R)(l \cos \theta)] \qquad (2.11)$$

where $\bar{h}$ can be taken either as the nominal or time averaged value of the strip thickness $h$. It is possible to express the strip angles $\alpha_L$ and $\alpha_R$ in terms of $\theta$:

$$- \cos \alpha_L + \cos \alpha_R = - \frac{d + l \cos \theta}{L_L} + \frac{D - d - l \cos \theta}{L_R} \qquad (2.12)$$

$$\sin \alpha_L + \sin \alpha_R = (l \sin \theta + r_l - y) \left( \frac{1}{L_L} + \frac{1}{L_R} \right) \qquad (2.13)$$

Loads caused by the strip and looper weights are, respectively:

$$M_s = \bar{h} w \rho g (L_L + L_R) l \cos \theta \qquad (2.14)$$

$$M_w = m_L g r_L \cos \theta \qquad (2.15)$$

A simple strength analysis (Appendix B) leads to Equation 2.16 for bending moment which resembles the one given by Hearns *et al.* [15].

$$M_b = \frac{4}{3} \frac{\sigma_y w \bar{h}^2}{D} l \cos \theta \qquad (2.16)$$

So the total looper load is:

$$M_L = M_\sigma + M_s + M_w + M_b \qquad (2.17)$$

Looper load is only a function of the strip tension $\sigma$ and looper angle $\theta$ then, provided that the strip dimensions, material and temperature remain the same.

Looper torque $M$ is delivered by the looper motor based on the torque reference signal $M_{ref}$ from the controller. Modeling the current regulator as a first order lag:

$$\frac{M(s)}{M_{ref}(s)} = \frac{1}{T_{cr}s + 1} \tag{2.18}$$

Equations obtained so far can be compactly written as:

$$\dot{\theta} = \omega_L \tag{2.19}$$

$$\dot{\omega}_L = \frac{1}{J(\theta)}(-M_L(\sigma, \theta) - M_F(\dot{\theta}) + M) \tag{2.20}$$

$$\dot{\sigma} = \frac{E}{L(\theta)}\left(\frac{dL}{d\theta}\omega_L - \mathbf{v} + \mathbf{V}_{i+1}\right) \tag{2.21}$$

$$\dot{M} = -\frac{M}{T_{cr}} + \frac{1}{T_{cr}}\mathbf{M}_{ref} \tag{2.22}$$

Taking the torque reference $M_{ref}$ and the strip speeds $v, V_{i+1}$ as the inputs, this is a nonlinear ODE set with 4 equations and 4 unknowns, namely the looper angle $\theta$, looper speed $\omega_L$, strip tension $\sigma$ and looper torque $M$.

## 2.3 Main Drive

The main drive as modeled here consists of a drive motor and rolls; gears, shafts and couplings that connect them, and the speed regulator which sets the motor torque.

Newton's law of motion can be written for the main drive:

$$J_{md}G_r\dot{\omega} = M_D - \frac{M_R}{G_r} \tag{2.23}$$

$J_{md}$ here is the total inertia of the drive motor, rolls and all mechanical parts connecting them, on motor side. $G_r$ is the ratio of the motor shaft angular displacement to the work roll angular displacement. Following Guo's main drive model [12], friction is omitted in Equation 2.23. Tessendorf [33] notes that it is common practice, at least in the design stage, to assume very low damping ratios for the main drives. Moreover, the damping factors given by Dhaouadi et al. [5] for a mini-model system are much lower than 0.1. Shaft stiffness is also neglected in this study.

With the speed regulator included, the block diagram of the drive system is like in Figure 2.2. The speed regulator could be a PI controller. Tessendorf simplifies the flux regulator
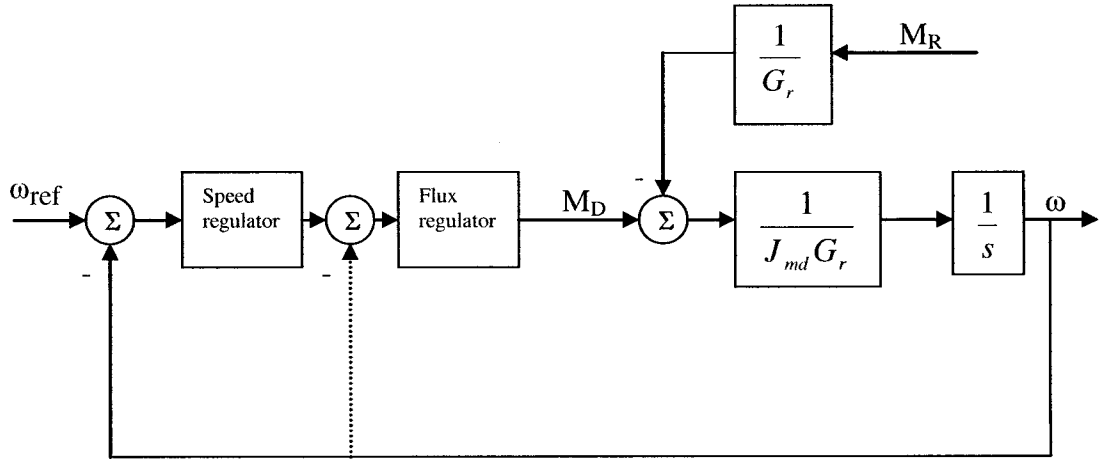


Figure 2.2: Simplified main drive system

as a gain and first order lag element. It is very fast and will be neglected here. With a PI controller as the speed regulator:

$$\dot{x}_c = \frac{K_c}{\tau_I}(\omega_{ref} - \omega) \tag{2.24}$$

$$\Delta M_D = x_c + K_c(\omega_{ref} - \omega) \tag{2.25}$$

where $K_c$ and $\tau_I$ are the regulator gain and integral time constants.

## 2.4 Roll Actuators

Roll actuators are either electromechanical screws or hydraulic systems. In some mills both are used, being installed on different stands. Detailed modeling of a hydraulic system is a complex task involving the studies of its individual parts such as servovalve, transmission line, hydraulic cylinder and so forth. Such detailed models can be found in [9] or [11]. Following Guo's cold mill model [12], a second order lag will be used here for both electromechanical and hydraulic actuator positions:

$$\frac{C(s)}{C_{ref}(s)} = \frac{1}{\tau_{pr_1}\tau_{pr_2}s^2 + \tau_{pr_2}s + 1} \tag{2.26}$$

with a different pair of time constants $\tau_{pr_1}$ and $\tau_{pr_2}$ for each. The roll force $F$ is not considered a significant disturbance on the actuator position.

Screw or piston position $C$ may be interpreted as the amount of roll gap under no load. Rolls are elastically deformed when the strip is between them, however, and the roll gap, which then becomes identical to exit strip thickness, may be expressed as:

$$h = C + \frac{F}{K_s} \tag{2.27}$$

The stand stiffness $K_s$ here is a lumped parameter accounting for the axial and local deformation of all rolls, mill housing and other mechanical parts involved.

## 2.5  Coiler

The coiler is a rotating mandrel around which the coil is wrapped to form a coil. The coiling operation should be performed under some tension to avoid loose coils which are commercially unacceptable. Newton's law of motion can be written for the coiler motor shaft as follows:

$$J_c \dot{\omega}_c = M_c - \sigma r_c \frac{w\bar{h}}{G_r} \tag{2.28}$$

where $J_c$ is the total inertia of the mandrel and coil as seen by the motor, and $G_r$ is the ratio of motor angular displacement to mandrel angular displacement. As the strip is wrapped around, both the coil radius $r_c$ and total inertia $J_c$ increase. Considering that one revolution of the mandrel should increase the coil radius by an amount equal to $\bar{h}$, the coil radius and total inertia can be expressed as:

$$\dot{r}_c = \frac{\omega_c}{2\pi G_r} \bar{h} \tag{2.29}$$

$$J_c = J_{c0} + \frac{\pi}{2} \frac{\rho w}{G_r^2} (r_c^4 - R_c^4) \tag{2.30}$$

Strip entry speed to the coil is simply:

$$V_c = \frac{\omega_c}{G_r} r_c \tag{2.31}$$

## 2.6 Transport Delay

The transport delay between stands applies to strip thickness and temperature, and it varies because of mill speedup and roll speed fluctuations. If the finishing mill were run at constant nominal speed, the transport delay might be considered constant under the assumption that the operation is smooth enough to neglect the effect of roll speed fluctuations. A general approach that accounts for both mill acceleration and speed fluctuations will be developed here.

It is obvious that the amount of strip $L(t_0)$ that exists between the stands at a moment $t_0$ when a specific point on the strip loses contact with the upstream stand must be consumed by the downstream stand in order for the point to reach the downstream stand. This can mathematically be described as:

$$L(t_0) = \int_{t_0}^{t_0+\tau_0} V_{i+1}\, dt \qquad (2.32)$$

The transport delay $\tau_0$ for the point appears in the upper limit of integration in Equation 2.32. The length $L_t$ to be threaded for the points emerging after time $t_0$ to reach the downstream stand (cumulative from the first point) is:

$$L_t(t) = L(t_0) + \int_{t_0}^{t} v\, dt \qquad (2.33)$$

The transport delay problem can be solved using a length coordinate instead of time and creating a buffer. The buffer should contain values of the delayed variables, strip length $L_t$ to be threaded for each value, and time of exiting the upstream stand, all in separate columns. Sampling rate could be adjusted according to the desired accuracy. This would create a table similar to the one given below:

| $k$ | $h$ | $T$ | $L_t$ | $t$ |
|-----|-----|-----|-------|-----|
| 1 | $h_1$ | $T_1$ | $L_1$ | $t_1$ |
| 2 | $h_2$ | $T_2$ | $L_1 + \int_{t_1}^{t_2} v\, dt$ | $t_2$ |
| 3 | $h_3$ | $T_3$ | $L_1 + \int_{t_1}^{t_3} v\, dt$ | $t_3$ |
| $\vdots$ | | | | |
| $n$ | $h_n$ | $T_n$ | $L_1 + \int_{t_1}^{t_n} v\, dt$ | $t_n$ |

It is also known at any time how much strip has been threaded by the downstream stand:

$$L_T(t) = \int_{t_1}^{t} V_{i+1} \, dt \tag{2.34}$$

Therefore it is possible to calculate the delayed thickness at any time by reading from the buffer the thickness corresponding to the value of Equation 2.34. An interpolation technique should be used for the values in between. This shows that it is not necessary to compute the delay time itself to handle the transport delay problem. If desired, however, it can be computed by reading from the buffer the time of leave $t_k$ and subtracting it from the current time. In fact it is necessary to do so in this case because, unlike the thickness, the temperature is not constant for a strip segment but decreases in time due to radiation whose effect depends on the amount of delay time.

## 2.7  Deformation

The force exerted on the roll by the deforming metal sheet is expressed as:

$$F = Kw\sqrt{R(H - h)} \tag{2.35}$$

The term $w\sqrt{R(H - h)}$ represents the contact area between the roll and the sheet; so the deformation resistance $K$ may be understood as a mean deformation pressure. It appears to be a general consensus to express the deformation resistance as the product of a geometric factor $Q$ and a mean yield stress $\bar{\sigma}$, although the nomenclature widely varies.

$$K = Q\bar{\sigma} \tag{2.36}$$

The geometric factor $Q$ is generally related to the inlet and exit gages $H$, $h$ and the deformed roll radius $R$ in various functional forms. It is another consensus to consider the mean yield stress $\bar{\sigma}$ as a function of strip temperature $T$, reduction $r = (H-h)/H$ (or often engineering stress $\epsilon = \ln H/h$), and the mean strain rate $\dot{\epsilon}$, which is a function of how fast the sheet is deformed.

Various methods, most being partly graphical, have been developed to predict the deformation resistance. A good summary of these methods can be found in [9]. It appears that a simple non-dimensional parameter named aspect ratio $z_a$ could be very useful to

describe the deformation phenomena. Ginzburg [8] remarks that it is possible to express the deformation resistance as a simple function of the temperature and aspect ratio, omitting the parameters such as reduction and strain rate. It is also discussed by Pietrzyk and Lenard [24], who use an inverse aspect ratio and name it the shape coefficient.

The method developed by Alexander and Ford and later modified by Gupta and Ford [13] has been preferred in this study. It has a simpler geometric factor depending on the aspect ratio only.

$$Q = \frac{1}{2}(\pi + z_a) = \frac{\pi}{2} + \frac{\sqrt{R(H-h)}}{H+h} \qquad (2.37)$$

Gupta and Ford give graphical representations of how mean shear yield stress $\bar{\sigma}$ changes with temperature and mean strain rate. The mean strain rate as defined by Alexander and Ford is:

$$\dot{\epsilon} = \omega\sqrt{\frac{R_0}{H}}\left(1 + \frac{r}{4}\right) \qquad (2.38)$$

The yield stress of the steel increases with increasing strain rate and decreasing temperature. The graphical form is not convenient for simulation purposes and a functional form has therefore to be experimentally determined.

$$\bar{\sigma}_o = \bar{\sigma}_o(T, \dot{\epsilon}) \qquad (2.39)$$

It is also known that the mean yield stress decreases with increasing strip tension. Hessenberg-Sims equation as presented by Shohet and Townsend [30] accounts for this in the following way, modified here to use the mean shear yield stress rather than the mean yield stress originally used:

$$\bar{\sigma} = \bar{\sigma}_o - \frac{1}{\sqrt{3}}\frac{\Sigma + \sigma}{2} \qquad (2.40)$$

The total deformation torque may be defined as:

$$M_R = 2Fa\sqrt{R(H-h)} + (R + h/2)(\Sigma_i \bar{H} - \sigma_i \bar{h})w \qquad (2.41)$$

The first term in Equation 2.41 is simply the multiplication of the roll forces with the length of the lever arm, expressed as a fraction $a$ of the contact length. The second term reflects the effect of strip tension. There are numerous equations for the lever arm factor $a$ in the literature. The expression presented by Pietrzyk and Lenard [24], rewritten here as a

function of the aspect ratio, is:

$$a = 0.594 z_a^{-0.3146} \tag{2.42}$$

Finally it should be remarked that the work roll radius $R$ used so far is the deformed roll radius and is related to the actual radius $R_0$ through Hitchcock's equation [9]:

$$R = R_0 \left( 1 + \frac{F}{(H-h)w} \frac{16(1-\nu_r^2)}{\pi E_r} \right) \tag{2.43}$$

Roll deformation becomes more severe at later stands where the reductions are smaller, lessening the contact area between the strip and the roll.

## 2.8  Heat Transfer

Temperature has a very significant effect on the deformation resistance and has to be predicted accurately. Conduction to the rolls and radiation in the inter-stand region are two main causes of heat loss. Convective loss to air is relatively insignificant [9, 27]. Sometimes the workpiece is also deliberately cooled by spraying water. Finally, the strip gains heat due to the mechanical work done by the rolls.

Ginzburg [9] provides a compilation of the available equations for each item listed above. Although the forms are similar, their predictions are substantially different. The main reason is the disagreement about how the total heat loss should be distributed among different heat transfer forms. The equations therefore have to be calibrated using plant data.

The equation derived by Ginzburg [8] for the temperature drop due to conduction can be rewritten in the following form with the addition of a calibration coefficient $b_1$:

$$\Delta T_c = b_1 \frac{8k}{\rho c} \frac{(T - T_r)}{H + h} \left( \frac{\sqrt{R_0(H-h)}}{\pi \alpha_r v} \right)^{1/2} \tag{2.44}$$

A dynamic computation of effective roll temperature $T_r$ is complex and costly because of the multi-dimensional heat transfer and the uncertainty brought in by roll cooling. Instead, it may safely be taken as a constant considering that $T_r$ is quite small compared to $T$ and the effective roll temperatures virtually remain constant once they reach steady state after a roll change.

Heat gain due to the work done by the rolls has generally been related to the deformation resistance and the true stress. A common form is [27]:

$$\Delta T_m = b_2 \frac{K}{\rho c} \ln \frac{H}{h}$$

(2.45)

where $b_2$ is the fraction of the work transformed into heat.

The amount of radiative loss is related to the transport delay $\tau$ between the stands. The strip exiting stand $i$ with a temperature $t_i$ arrives at stand $i + 1$ at a temperature $T_{i+1}$, which can easily be shown to be equal to:

$$T_{i+1} = \left( b_3 \frac{6S\epsilon}{\rho \bar{h} c} \tau_i + \frac{1}{t_i^3} \right)^{-1/3}$$

(2.46)

$b_3$ here is a calibration parameter to account for the uncertainty in strip thermal properties. The stand exit temperature $t_i$ in Equation 2.46 is simply:

$$t_i = T_i - \Delta T_c + \Delta T_m$$

(2.47)

Inter-stand cooling is not modeled in this study. Temperature drops due to inter-stand cooling will be assumed constant.

## 2.9  Slip

Slip is a difference between the work roll peripheral speed and the strip speed. Strip speed fluctuation is the main disturbance on the looper-strip system; so it is crucial to grasp adequately its dependence on many factors such as inlet and exit gage or tension.

As part of their study on cold rolling with strip tension, Ford et al. [7] develop Siebel's theory of rolling so that it can be applied to cases of rolling with strip tension. The forward slip equation derived using this extended theory has been employed by Hitachi researchers Eto et al. [6] in a slightly simplified form for design of an automatic tension and gage control system at a tandem cold mill. The relationships given by Ford et al. can be combined to obtain the following expression for forward slip factor $f$:

$$f = \frac{R}{h} \left( \frac{1}{2} \sqrt{\frac{H-h}{R}} - \frac{\sqrt{3}\bar{\sigma}(H-h) + H\Sigma - h\sigma}{4\sqrt{3}\bar{\sigma}R\mu} \right)^2$$

(2.48)

where $\sqrt{3}$ is a correction factor to convert mean shear yield stress $\bar{\sigma}$ used in this study to mean yield stress in the original derivation. The basic set of equations employed by Moon *et al.* [20] to predict the forward slip in case of hot rolling can also be shown to yield the same expression with Equation 2.48 after some simplifications.

The friction coefficient $\mu$ in Equation 2.48 is a function of temperature and roll speed, as well as of the materials involved and lubrication conditions. It can be estimated from forward slip measurements, but forward slip is difficult to measure directly. Moon *et al.* [20] make use of the correlation between the friction coefficient and rolling torque to estimate the friction coefficient and find that for a 7-stand hot mill, its value is in the range 0.15-0.2. Since no other data is available, a representative value of 0.2 will be used in this study.

Stand exit strip speed $v$ is related to the forward slip factor as follows:

$$v = \omega R_0(1 + f) \tag{2.49}$$

Inlet strip speed $V$ can then be calculated considering the mass balance:

$$V = \frac{vh}{H} \tag{2.50}$$

## 2.10  Model Completeness Analysis

The complexity and large number of equations make it more convenient to carry out a block diagram analysis. The analysis will be performed for a single stand and then the results will be generalized for the whole finishing mill. A more rigorous analysis is given in Chapter 3 which deals with the linearization problem. A summary of model equations can be found in Appendix C.

Disturbances reaching a particular stand originate either from the upstream or downstream stands. Incoming thickness $H$, temperature $T$ and back strip tension $\Sigma$ belong to the first group. The major disturbance originating from the downstream stand is its strip entry speed $V_{i+1}$. The vector of disturbances on Stand i may therefore be defined as:

$$\mathbf{w} = [\ \Sigma \quad H \quad T \quad V_{i+1}\ ]^T \tag{2.51}$$

All these disturbances are shown in Figure 2.1.

As modeled here, a finishing mill stand has three control inputs: the main drive speed reference $\omega_{ref}$, looper torque reference $M_{ref}$ and roll position reference $C_{ref}$. The control vector is:

$$\mathbf{u} = [\ \omega_{ref} \quad M_{ref} \quad C_{ref}\ ]^T \tag{2.52}$$

If the model equations constitute a complete set, with inputs $\mathbf{w}$, $\mathbf{u}$ and necessary initial conditions for the differential equations, they should be able to produce the outputs that will be disturbances to other stands in case the stands are linked end-to-end to form the finishing train. It is possible to see from the flow chart presented in Figure 2.3 that this condition is satisfied. Numbers given in the blocks are the numbers of the associated equations. It is seen in Figure 2.3 that the disturbances to the downstream stand, namely $\Sigma_{i+1}, H_{i+1}$ and $T_{i+1}$ and the disturbance $V$ affecting the upstream stand can be calculated from the model equations. This proves that if the stands are connected to each other, there will be a seamless flow of disturbance variables and no external variables will have to be supplied apart from the control inputs. Only the thickness, temperature and back strip tension for Stand 1 and downstream strip speed for Stand 7 will be necessary. The disturbance vector for the whole mill is then:

$$\mathbf{W} = [\ \Sigma_1 \quad H_1 \quad T_1 \quad V_c\ ]^T \tag{2.53}$$

$V_c$ in $\mathbf{W}$ is the strip entry speed to coiler, which becomes the downstream strip speed for Stand 7. If the coiler is also included in the model, there will be no need to supply it externally and $\mathbf{W}$ will become 3 by 1. Finally it should be noted that back strip tension $\Sigma_1$ is always zero excluding the short intervals when the crop shear operates.
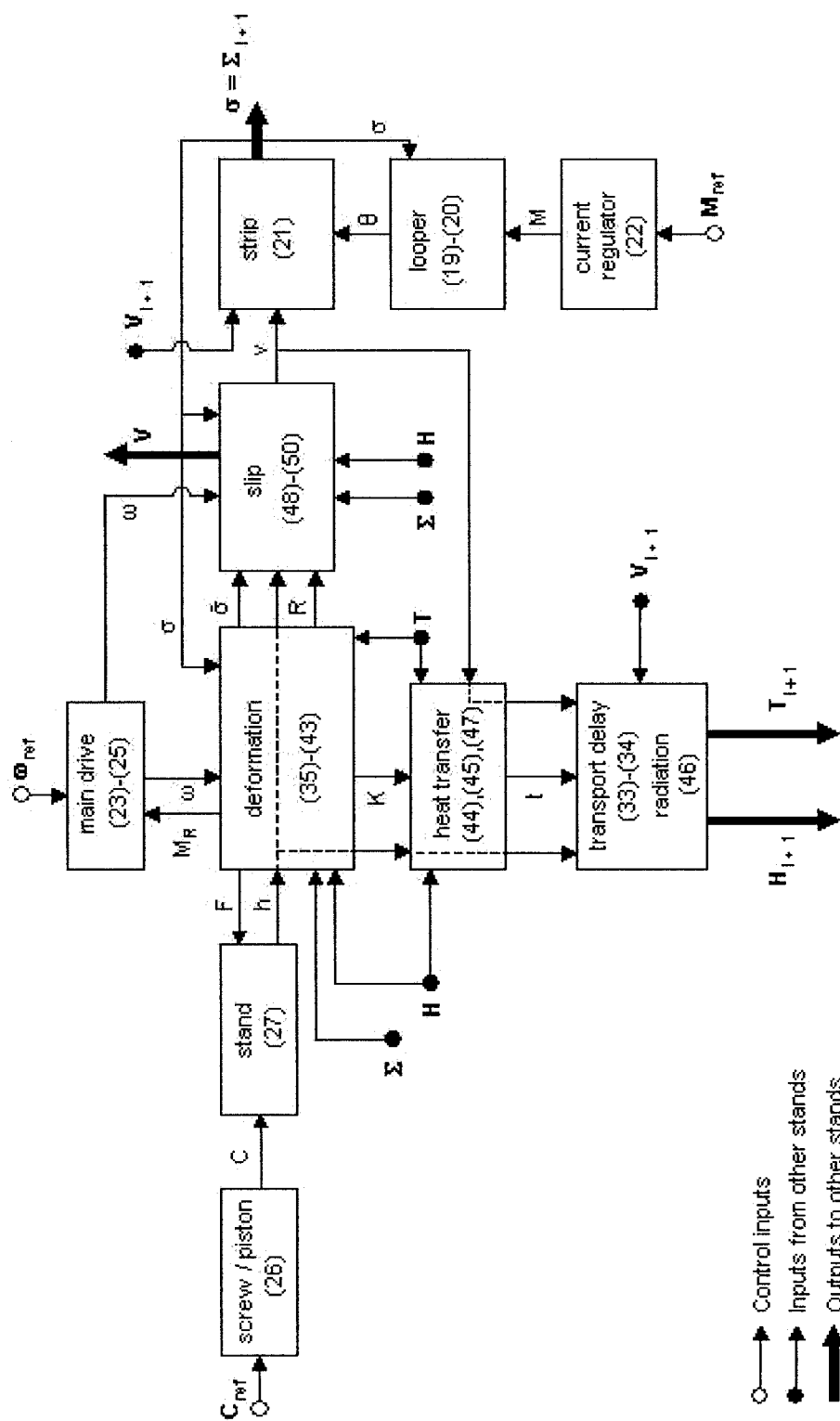
Figure 2.3: Block diagram showing the interactions of Stand i

*"Here we have a state whose subjects are so happy that they have to be forbidden to quit its bounds under the direst penalties."*

— Churchill on Russia, 1919

# 3

# Linear State-Space Form

A finishing mill stand is represented by a set of nonlinear differential and algebraic equations (DAE's). If linearized, however, these two sets of equations can be reduced to a simple set of ordinary differential equations (ODE's). It is also possible, after some matrix manipulations, to describe the whole finishing mill as a set of ODE's. Existence of such a set will constitute a more rigorous proof that the solution of the model equations is feasible.

## 3.1  State-Space Representation of a Single Stand

In order to obtain a linear state-space form of the stand equations, dynamic and algebraic states should be defined and the equations should be linearized. They can then be assembled utilizing the control and disturbance vectors, u and w, which have previously been defined in Section 2.10. In this study the transport delays will be handled through Padé approximations and each delay will be included in the equation set of its upstream stand.

30

### 3.1.1 Dynamic states

Equations 2.19-2.22 describe the motion of the strip and looper. After removing the static friction term which is impossible to linearize, these equations can be linearized without further simplifications. Main drive and roll actuator dynamics, however, will be simplified to keep the system order low. Equations 2.23-2.25 and 2.26 are hence reduced to, respectively:

$$\frac{\omega(s)}{\omega_{ref}(s)} = \frac{1}{T_{md}\ s + 1} \tag{3.1}$$

$$\frac{C(s)}{C_{ref}(s)} = \frac{1}{T_{pr2}\ s + 1} \tag{3.2}$$

The delayed thickness $H_{i+1}$ and temperature $T_{i+1}$ can be expressed using first order Padé approximations:

$$\frac{H_{i+1}(s)}{h(s)} = \frac{-\tau/2\ s + 1}{\tau/2\ s + 1} \tag{3.3}$$

$$\frac{T_{i+1}(s)}{t_R(s)} = \frac{-\tau/2\ s + 1}{\tau/2\ s + 1} \tag{3.4}$$

$t_R$ is a non-physical variable which has the same magnitude with $T_{i+1}$ and is in phase with $t$, the exit temperature of the strip from the stand. Equations 3.3 and 3.4 are converted to their state-space forms by introducing two new states $p$ and $n$.

$$\dot{p} = -2/\tau\ p + 2/\tau\ h \tag{3.5}$$

$$\dot{n} = -2/\tau\ n + 2/\tau\ t_R \tag{3.6}$$

$$H_{i+1} = 2p - h \tag{3.7}$$

$$T_{i+1} = 2n - t_R \tag{3.8}$$

The state vector x has altogether 8 variables now, which are:

$$\mathbf{x} = \begin{bmatrix} \theta & \omega_L & \sigma & p & n & \omega & M & C \end{bmatrix}^T$$

Linearizing Equations 2.19-2.22, the rest being linear already, a linear state-space representation is possible:

$$\dot{\mathbf{x}} = A\mathbf{x} + B_1 \begin{bmatrix} \omega_{ref} \\ M_{ref} \\ C_{ref} \end{bmatrix} + B_2 \begin{bmatrix} v \\ h \\ t_R \end{bmatrix} + B_3 V_{i+1} \tag{3.9}$$

where

$$A = \begin{bmatrix} \frac{\partial \dot{\omega}_L}{\partial \theta} & -\frac{c_f}{J} & 1 & -\frac{1}{J}\frac{\partial M_L}{\partial \sigma} & & & & \frac{1}{J} \\ \frac{\partial \dot{\sigma}}{\partial \theta} & \frac{E}{L}\frac{dL}{d\theta} & & & & & & \\ & & & -\frac{2}{\tau} & & & & \\ & & & & -\frac{2}{\tau} & & & \\ & & & & & -\frac{1}{T_{md}} & & \\ & & & & & & -\frac{1}{T_{cr}} & \\ & & & & & & & -\frac{1}{T_{pr2}} \end{bmatrix}_{(8,8)}$$

$$B_1 = \begin{bmatrix} & & \\ & & \\ \frac{1}{T_{md}} & & \\ & \frac{1}{T_{cr}} & \\ & & \frac{1}{T_{pr2}} \end{bmatrix}_{(8,3)} \qquad B_2 = \begin{bmatrix} -\frac{E}{L} \\ \frac{2}{\tau} \\ & \frac{2}{\tau} \end{bmatrix}_{(8,3)} \qquad B_3 = \begin{bmatrix} \frac{E}{L} \\ \\ \\ \end{bmatrix}_{(8,1)}$$

Note that in Equation 3.9 the vector consisting of the reference inputs is actually the control vector $\mathbf{u}$, the vector with coefficient $B_2$ is formed purely by some algebraic variables of the stand itself, and $V_{i+1}$ is a component of the disturbance vector $\mathbf{w}$.

## 3.1.2 Algebraic states

The number of the algebraic states is arbitrary because most of the algebraic equations may be substituted into each other and the overall number may change. For convenience $v, h$ and $t_R$ should be kept, however, because they appear in Equation 3.9. As obvious from Equations 3.7 and 3.8, $H_{i+1}$ and $T_{i+1}$ should also be included. Together with some other variables whose direct tracking is desirable, the 13 element algebraic state vector is:

$$\mathbf{s} = \begin{bmatrix} v & H_{i+1} & T_{i+1} & V & h & t_R & F & K & \bar{\sigma} & f & t & M_R & R \end{bmatrix}^T$$

Interactions between these variables and numbers of the equations involved are shown on the block diagram in Figure 2.3. After linearization, they can be expressed as:

$$\mathbf{s} = C\mathbf{s} + D_1 \begin{bmatrix} \Sigma \\ H \\ T \end{bmatrix} + D_2 \begin{bmatrix} \sigma \\ p \\ n \\ \omega \\ C \end{bmatrix} \qquad (3.10)$$

where

$$C = \begin{bmatrix}
 & & & & & & & & & \omega R_0 & & & \\
 & -1 & & & & & & & & & & & \\
 & & & -1 & & & & & & & & & \\
 \frac{h}{H} & & \frac{v}{H} & & & & & & & & & & \\
 & & & & \frac{1}{K_s} & & & & & & & & \\
 & & & & & & (t_R)_t & & & & & & \\
 & F_h & & & & F_K & & & & & F_R & & \\
 & K_h & & & & & K_{\bar\sigma} & & & & K_R & & \\
 & \bar\sigma_h & & & & & & & & & & & \\
 & f_h & & & & & f_{\bar\sigma} & & & & f_R & & \\
 t_v & t_h & & & & t_K & & & & & & & \\
 & (M_R)_h & & (M_R)_F & & & & & & & (M_R)_R & & \\
 & R_h & & R_F & & & & & & & &
\end{bmatrix}_{(13,13)}$$

$$D_1 = \begin{bmatrix}
 & & \\
 & -\frac{vh}{H^2} & \\
 & & \\
 & F_H & \\
 & K_H & \\
 -\frac{1}{2\sqrt{3}} & \bar\sigma_H & \bar\sigma_T \\
 f_\Sigma & f_H & \\
 & t_H & t_T \\
 (M_R)_\Sigma & (M_R)_H & \\
 & R_H &
\end{bmatrix}_{(13,3)}
\qquad
D_2 = \begin{bmatrix}
 & & & R_0(1+f) & \\
 & 2 & & & \\
 & & 2 & & \\
 & & & & 1 \\
 & & & & \\
 -\frac{1}{2\sqrt{3}} & & & \bar\sigma_\omega & \\
 f_\sigma & & & & \\
 (M_R)_\sigma & & & &
\end{bmatrix}_{(13,5)}$$

and the variables with subscripts are the appropriate partial derivatives.

It should be remarked that in Equation 3.10, the vector with coefficient $D_1$ is a part of the disturbance vector w and the vector with coefficient $D_2$ is a part of the state vector x.

### 3.1.3  Reduction to ODE form

The control vector u and the disturbance vector w have previously been defined in Section 2.10. Repeating here for convenience, they are:

$$\mathbf{u} = \begin{bmatrix} \omega_{ref} & M_{ref} & C_{ref} \end{bmatrix}^T$$

$$\mathbf{w} = \begin{bmatrix} \Sigma & H & T & V_{i+1} \end{bmatrix}^T$$

It is not hard to see that both Equations 3.9 and 3.10 can be written in terms of the 4 standard vectors that have been defined so far, namely the dynamic and algebraic state vectors, the control vector, and the disturbance vector. Hence Equation 3.9 and 3.10 become, respectively:

$$\dot{x} = Ax + Bu + Gs + Hw \tag{3.11}$$

$$s = Cs + Dw + Lx \tag{3.12}$$

Above, $A$ and $C$ remains the same with those of Equations 3.9 and 3.10. $B$ is simply $B_1$, and rest of the coefficients, $G, H, D$ and $L$ can easily be created using columns of matrices $B_2, B_3, D_1$ and $D_2$, in the written order.

The DAE set can now be transformed into an ODE set. The solution of Equation 3.12 is:

$$s = (I - C)^{-1}(Dw + Lx) \tag{3.13}$$

The matrix $(I - C)$ has been found to be invertible for the range of operating conditions studied in this thesis. Equation 3.13 can be substituted into Equation 3.11 to yield, with a regrouping of terms:

$$\dot{x} = (A + G(I - C)^{-1}L)x + Bu + (H + G(I - C)^{-1}D)w \tag{3.14}$$

A more compact form would be, with an appropriate match of the coefficients:

$$\dot{x} = Ax + Bu + Hw \tag{3.15}$$

$$s = Lx + Dw \tag{3.16}$$

Thus the algebraic states have been eliminated and the stand dynamics has been directly related to external inputs, i.e. the control input and the disturbances.

## 3.2  State-space Representation of the Entire Mill

State-space representation of the whole plant is straightforward after one recognizes that the only disturbance in Equation 3.9, $V_{i+1}$, is actually an algebraic state of the next stand. So Equation 3.9 (or Equation 3.11) can be written in the following form for any stand $i$:

$$\dot{x}_i = A_i x_i + B_i u_i + G_i s_i + P_i s_{i+1} \tag{3.17}$$

$P_i$ is a sparse matrix made of $B_3$. It should be noted that $s_8$ does not exist and the term $P_i s_{i+1}$ in Equation 3.17 will be replaced by $H_7 W$ for stand 7. $W$ is the plant disturbance vector as defined in Section 2.10 and $H_7$ is the same with matrix $H$ in Equation 3.11.

Writing Equation 3.17 for all stands and stacking everything:

$$\dot{X} = A_p X + B_p U + G_p S + H_p W \qquad (3.18)$$

where $X = \begin{bmatrix} x_1 & \cdots & x_7 \end{bmatrix}^T_{(53,1)}$, $U = \begin{bmatrix} u_1 & \cdots & u_7 \end{bmatrix}^T_{(20,1)}$,
$S = \begin{bmatrix} s_1 & \cdots & s_7 \end{bmatrix}^T_{(91,1)}$ and

$$A_p = \begin{bmatrix} A_1 & & \\ & \ddots & \\ & & A_7 \end{bmatrix}_{(53,53)} \qquad B_p = \begin{bmatrix} B_1 & & \\ & \ddots & \\ & & B_7 \end{bmatrix}_{(53,20)}$$

$$G_p = \begin{bmatrix} G_1 & P_1 & & & \\ & G_2 & P_2 & & \\ & & \ddots & \ddots & \\ & & & G_6 & P_6 \\ & & & & G_7 \end{bmatrix}_{(53,91)} \qquad H_p = \begin{bmatrix} & \\ & \\ & \\ & \\ H_7 \end{bmatrix}_{(53,4)}$$

The 3 element deficit in $X$ and 1 element deficit in $U$ are caused by Stand 7, which does not have a looper and, consequently, the variables $\theta, \omega_L, M$ and $M_{ref}$, respectively.

A similar procedure is required for the algebraic equations. The disturbances in Equation 3.10 are some dynamic and algebraic states of the previous stand. Then, Equation 3.10 (or Equation 3.12) can be rewritten as:

$$s_i = C_i s_i + E_i s_{i-1} + F_i x_{i-1} + L_i x_i \qquad (3.19)$$

$E_i$ and $F_i$ can be made of $D_i$. As no $s_0$ or $x_0$ exists, the related terms will be replaced with $D_1 W$ for Stand 1. $D_1$ is the same matrix with the one in Equation 3.12.

Again stacking the individual stand equations:

$$S = C_p S + L_p X + D_p W \qquad (3.20)$$

Above,

$$C_p = \begin{bmatrix} C_1 & & & & \\ E_2 & C_2 & & & \\ & E_3 & C_3 & & \\ & & \ddots & \ddots & \\ & & & E_7 & C_7 \end{bmatrix}_{(91,91)} \qquad L_p = \begin{bmatrix} L_1 & & & & \\ F_2 & L_2 & & & \\ & F_2 & L_3 & & \\ & & \ddots & \ddots & \\ & & & F_7 & L_7 \end{bmatrix}_{(91,53)}$$

$$D_p = \begin{bmatrix} D_1 \\ \\ \\ \\ \\ \\ \end{bmatrix}_{(91,4)}$$

The solution to Equation 3.20 is:

$$\mathbf{S} = (I - C_p)^{-1}(L_p\mathbf{X} + D_p\mathbf{W}) \qquad (3.21)$$

The algebraic states vector $\mathbf{S}$ can be eliminated from Equation 3.18 via substitution of Equation 3.21. A regrouping of terms results in:

$$\dot{\mathbf{X}} = [A_p + G_p(I - C_p)^{-1}L_p]\mathbf{X} + B_p\mathbf{U} + [H_p + G_p(I - C_p)^{-1}D_p]\mathbf{W} \qquad (3.22)$$

or in a less bulky fashion:

$$\dot{\mathbf{X}} = \mathbf{A_p}\mathbf{X} + \mathbf{B_p}\mathbf{U} + \mathbf{H_p}\mathbf{W} \qquad (3.23)$$

$$\mathbf{S} = \mathbf{L_p}\mathbf{X} + \mathbf{D_p}\mathbf{W} \qquad (3.24)$$

Existence of the form shown in Equations 3.23 and 3.24 obviously depends on the invertibility of matrix $(I - C_p)$ and at the same time assures the feasibility of the solution. This matrix has been found non-singular for the operating conditions studied in this thesis. It is true that matrix $C_p$ changes with mill dimensions or steel properties but these changes may only be minor in size. Besides, the equations have physical origins so singularity should not be a problem as long as realistic mill conditions are studied.

## 3.3 Linear Model Performance

The linear model has a series of drawbacks compared to the full and nonlinear version. These may be ranked as follows:

1. The mill cannot be accelerated because this changes the transport delay, which cannot be approximated in a linear model. In a real operation mill speed may nearly double, hence almost halving the delay.

2. Disturbances with linear trends or large deviations will result in inaccurate solutions. One such disturbance is the mill inlet temperature, which decreases throughout the operation due to radiative heat loss.

3. Inevitable simplifications such as removal of the static friction term or Padé approximations for constant transport delays will introduce some inaccuracy, although not as severely as in cases 1 or 2.

In order to see what the linear model may do at best then, a comparison should be made using a constant mill speed and disturbances without trends. Results of such a comparison are presented in Figures 3.1 and 3.2. Sinusoidal entry temperature and gage profiles with respective amplitudes of 5° C and 0.1 mm and frequencies of 0.06 Hz and 0.2 Hz are used as disturbances. The differences seen in Looper 1 angle and strip tension in Figure
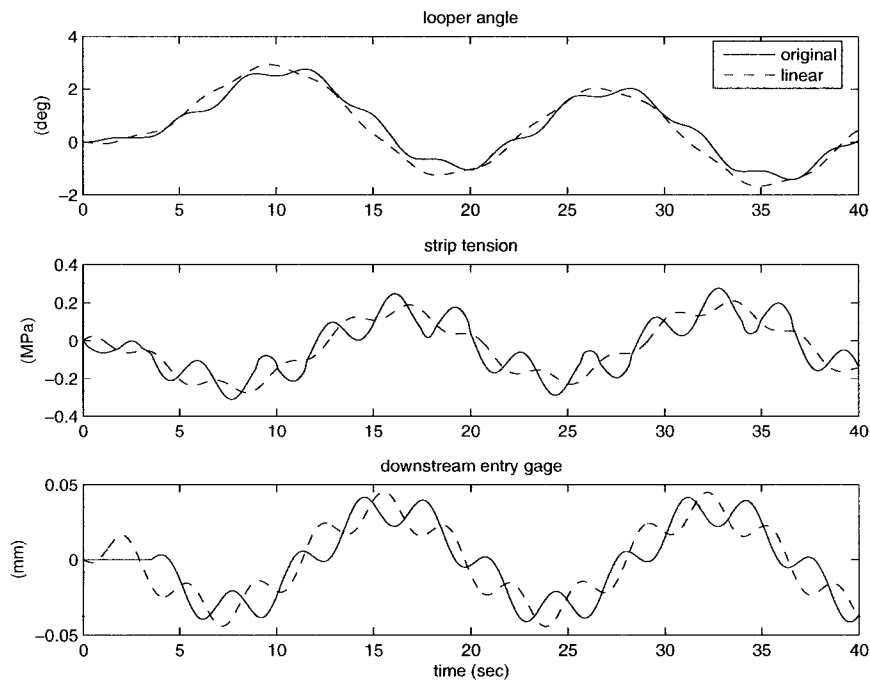
Figure 3.1: Linear model performance for Looper 1

3.1 are mainly because the static friction term cannot be included in the linear model. A looper system with more friction will naturally cause a larger tension fluctuation. It is also observed in Figure 3.1 that the first order Padé approximation is erroneous especially for high frequency changes. Results for Looper 5 is better as seen in Figure 3.2 owing to the very low static friction on this looper and the fact that only the temperature disturbance, which has a low frequency, is able to reach so far as Stand 5.
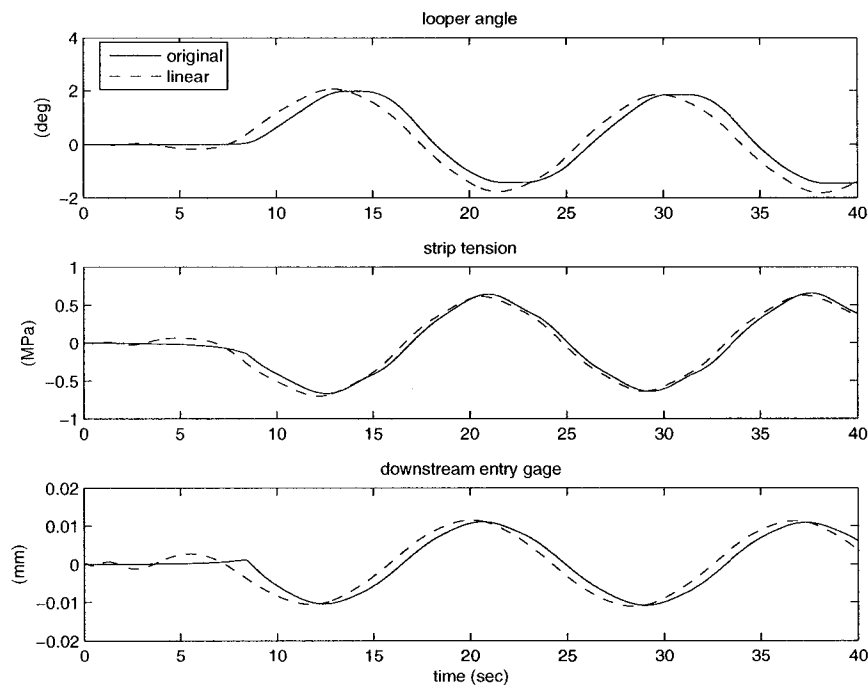


Figure 3.2: Linear model performance for Looper 5

A linear change may be added to the existing temperature profile to observe the consequences of a significant deviation from the original operating point. Results for a total added change of 12°C is presented in Figure 3.3. It is apparent here that looper-strip dynamics significantly changes when the deviations are large enough. The model linearized around the operating point is stable and will remain so independent of the deviation size whereas the looper system is in reality unstable at large angles where it simply becomes an inverted pendulum. This also points out that linear controllers cannot stabilize the system unless the looper angle is included among controlled variables and thus restricted.
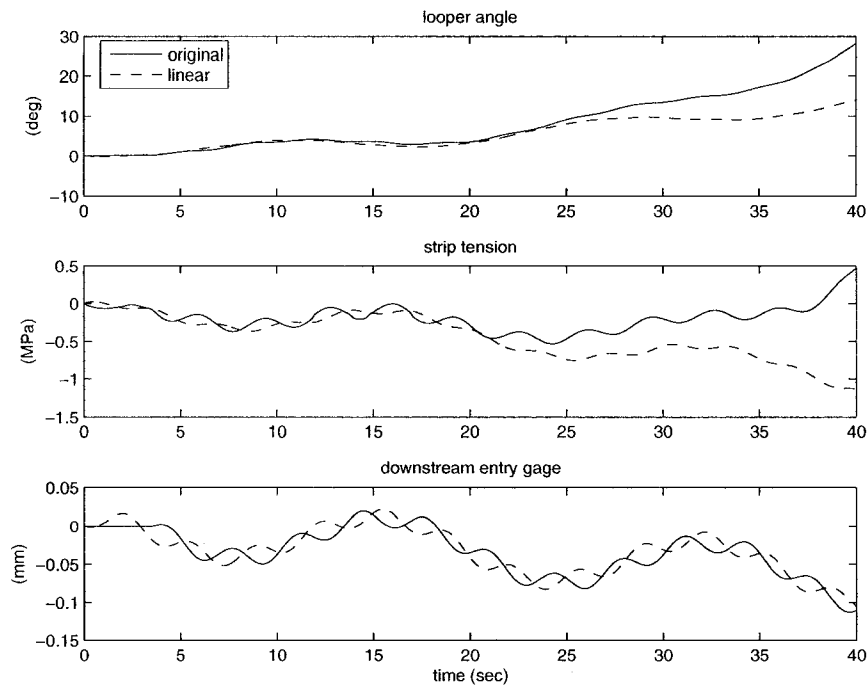
Figure 3.3: Linear model performance for Looper 1 in case of a disturbance with a linear trend.

Finally it should be noted that the analysis so far have been carried out for an uncontrolled plant. The variables are not expected to deviate as largely in the controlled case and the linear model may still perform comparably to some extent provided that the mill is not accelerated; however, its inability to simulate the variable transport delay cannot be removed. Simulation packages are necessary to overcome this problem and also to keep the nonlinearities.

*"Golf is a game whose aim is to hit a very small ball into an even smaller hole, with weapons singularly ill designed for the purpose."*

– Churchill

# 4

# Frequency Response and Control Design

Disturbances affecting a finishing mill span a wide frequency range and it is important to investigate the frequency response of the looper system to be able to judge the significance of a particular disturbance. A general discussion about the disturbances has been given in Section 1.5. More detailed and quantitative information can be found in Chapter 5. These will make it possible to specify the frequency band where the control action is required and can be effective.

Control design involves two major tasks: Design of a conventional looper control system and application of covariance control theory to looper control problem. The conventional system as described in section 1.6.1 is easy to design and will facilitate better understanding of finishing mill control problems as a preparation for more advanced control applications. It will also serve as a base case to which the covariance controller can be compared.

## 4.1  Looper Frequency Response

A look at Equations 2.19-2.22 reveals that the effective disturbance on a looper is the strip speed imbalance $V_{i+1} - v$. Essentially all disturbances on a stand, be it an inlet gage or temperature fluctuation, or roll eccentricity, manifest themselves in form of strip speed

40

fluctuations by changing the amount of slip. The means available to manipulate the looper are the roll speed $\omega$, which directly effects the looper position by changing the strip length, and the looper motor torque $M$.

The linear stand model in Equation 3.15 is not suitable for purposes of the investigation here because it considers the looper-gage interaction and thus would require knowledge of the gage control system, whose structure is often complex and uncertain. It would also cause a loss of generality of the analysis. Instead, the interaction may be regarded as a disturbance contributing to the strip speed imbalance $V_{i+1} - v$. Thus, a linear model in the following form can be derived (Appendix D):

$$\dot{x} = Ax + B_u \begin{bmatrix} \omega_{ref} \\ M_{ref} \end{bmatrix} + B_w \Delta V \tag{4.1}$$

where the state vector $x = \begin{bmatrix} \theta & \omega_L & \sigma & \omega & M \end{bmatrix}^T$; and $\Delta V$ is a general term for all speed disturbances including slip changes and downstream stand speed change.
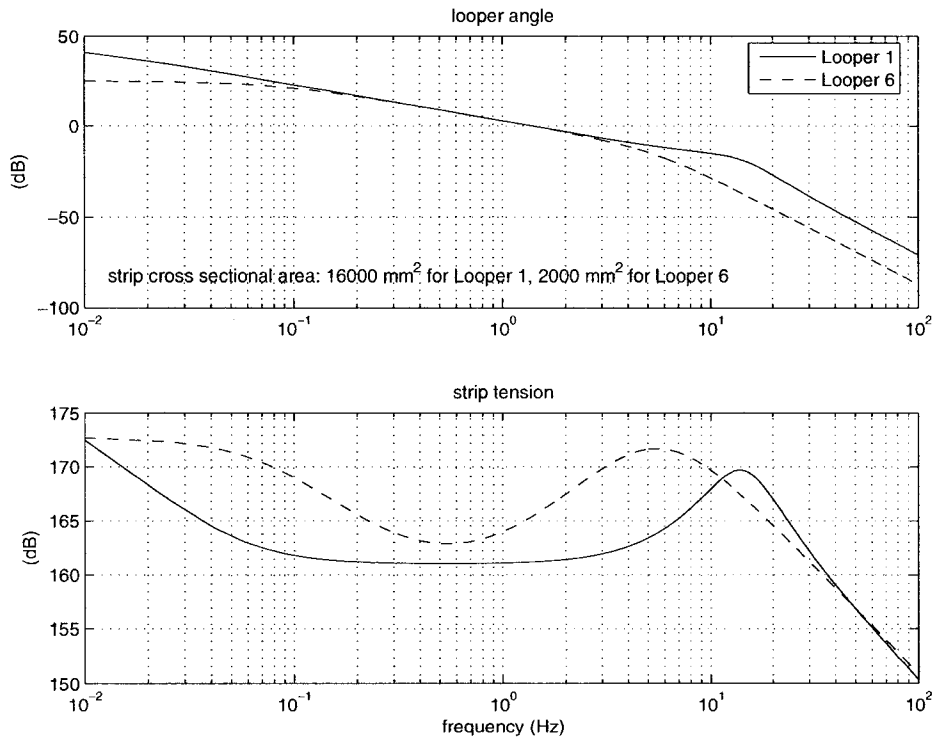


Figure 4.1: Sensitivities of Loopers 1 and 6 to speed disturbances

Since looper control is a regulation problem, a natural investigation will be how looper angle and strip tension are affected by the strip speed disturbance $\Delta V$. Angle and tension

responses of Loopers 1 and 6, which represent the two extreme cases with largest and smallest strip cross sectional areas, are shown in Figure 4.1. It is seen in Figure 4.1 that tension is very sensitive to high frequency disturbance which does not affect looper position significantly. This is expected because if the looper does not move, it cannot have any regulatory effect on tension. Another observation is the higher resonance frequency of Looper 1 at 14 Hz as opposed to roughly 5 Hz of Looper 6. The reason for this is the thinner strip at Looper 6. The lower resonance frequencies of later loopers point out that these are more difficult to control than the earlier loopers. Finally, the relatively flat gain of Looper 6 in Figure 4.1 at low frequencies should be attributed to its larger sensitivity to slip changes due to high stand speed there.

In order to determine how much control can be achieved, it is necessary to know the effect of the reference inputs on the controlled variables. Figures 4.2 and 4.3 show the responses of both outputs to stand speed reference $\omega_{ref}$ and looper torque reference $M_{ref}$, respectively. An immediate observation is that effectiveness of both inputs quickly
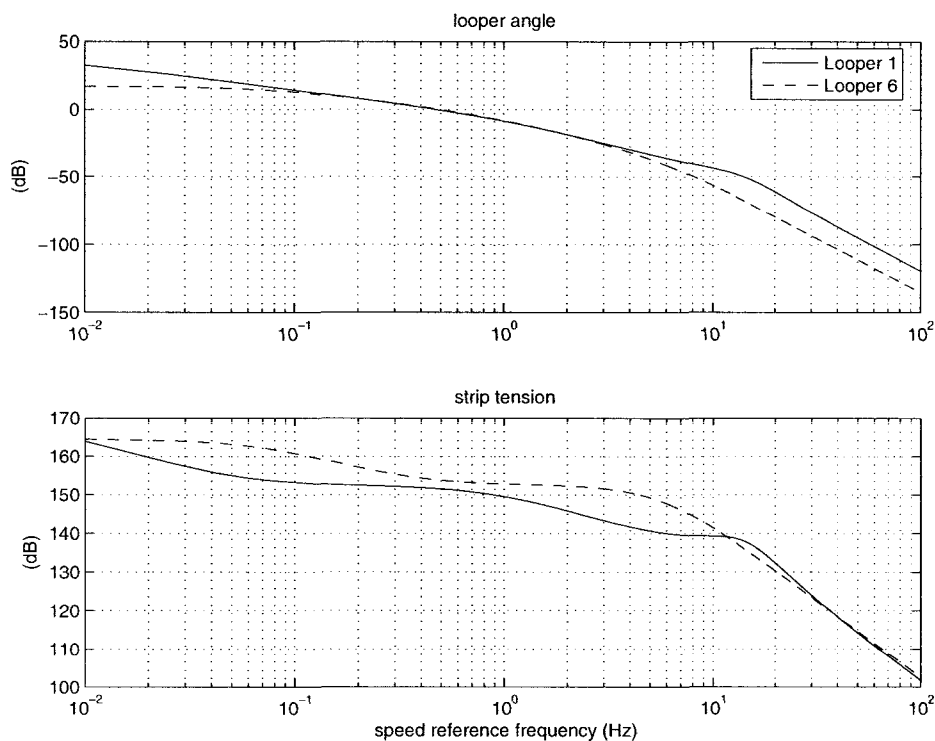


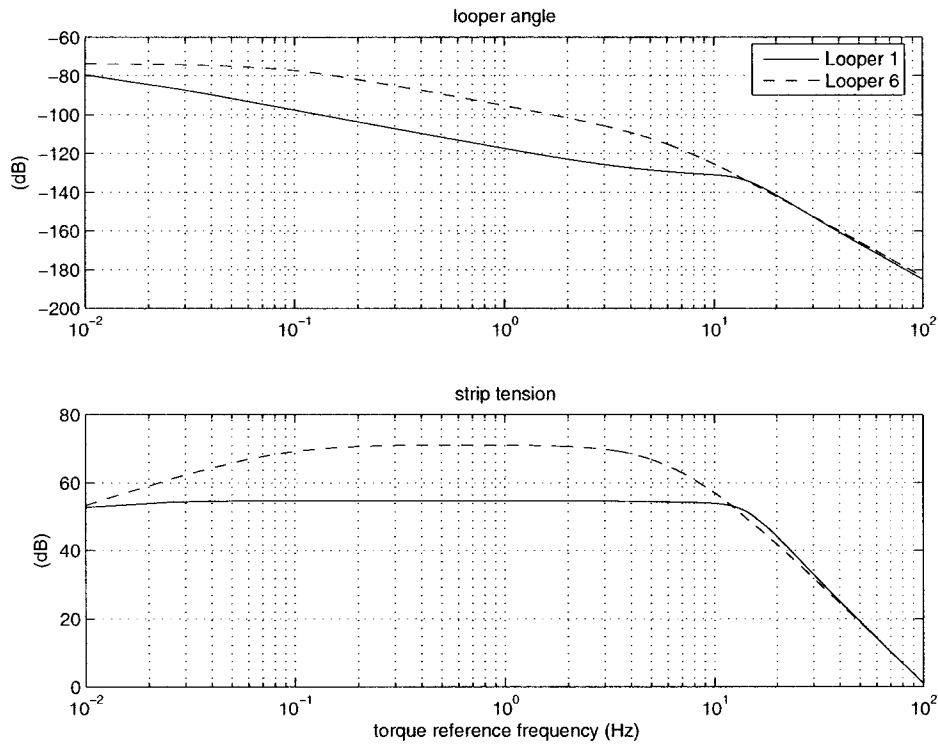Figure 4.2: Responses of Loopers 1 and 6 to stand speed reference input

Figure 4.3: Responses of Loopers 1 and 6 to looper torque reference input

disappears after the respective resonance frequencies of the loopers. Any attempt to exercise control around the resonance frequencies may demand an unreasonable amount of input. This is especially a problem for tension which keeps its sensitivity to disturbances well after the resonance frequency. It is also observed in Figure 4.3 that looper motor torque has a very weak effect on looper position. This is because the steel strip is a very stiff material and hard to stretch. Thus, the stand speed is a very effective control input on both outputs; whereas the torque in most cases can only wield influence on tension.

The higher sensitivity of the later loopers to strip speed disturbances has important consequences. As the later stands have higher rotation speeds due to the thinner strip with them, they introduce eccentricity disturbances at higher frequencies than the earlier stands do; hence exacerbating the situation. These stands are also equipped with hydraulic gage controllers which can act very quickly and may not exist on the earlier stands. Consequently, later loopers may receive disturbances near or above their resonance frequencies. Moreover, mill acceleration can reach a total of 50%, causing a general

rise in disturbance frequencies. Discussions so far indicate the importance of looper-strip resonance frequency. It was also discussed by Clark *et al.* [3] as the upper limit to the frequency of the mass flow disturbances the looper can handle. Being the effective determiner of the control bandwidth, it deserves detailed investigation, which follows next.

### 4.1.1 Looper-strip resonance frequency

Because the looper-strip system is weakly damped, the resonance frequency is essentially the same with the natural frequency, which can be extracted from Equations 2.19-2.21 as (Appendix D):

$$\omega_n \approx \sqrt{\frac{whE}{J}}\ \varphi_0 \tag{4.2}$$

where $\varphi_0$ is a function of system's geometric properties. The immediate conclusions that can be drawn from Equation 4.2 are:

1. The natural frequency is directly proportional to the square root of strip cross sectional area $wh$.

2. It is also directly proportional to the square root of strip elastic modulus $E$.

3. It is inversely proportional to the square root of system inertia $J$.

Thus, the effect of strip cross sectional area, which was apparent in Figure 4.1 has been quantified.

It is not possible to improve looper performance via Items 1 and 2, since these are determined by customer order and cannot be changed. Item 3, however, can be affected by decreasing the looper roll mass, motor and gear inertia, or altering the looper arm length. Modern loopers are generally directly driven to eliminate the gear inertia. For these modern designs Equation 4.2 can be further simplified to:

$$\omega_n \approx \sqrt{\frac{whE}{m_r}}\ \varphi \tag{4.3}$$

which indicates that the looper roll mass $m_r$ is the main determiner in such cases. The aforementioned conclusions are in accordance with those of [3, 4]. It is not easy to comment on the effect of looper arm length because a change in looper arm length may require a redesign of the whole system on which the function $\varphi$ depends.

## 4.2 Conventional Looper Control Design

Conventional looper control has two independent loops, both of which have been discussed in §1.6.1. The first loop regulates the looper angle by manipulating the upstream stand speed. To decouple the looper from the downstream stand, the speed reference signal from this stand is used in feedforward mode to correct the upstream stand speed. The second loop of the conventional system is for tension control. The torque change necessary to obtain the desired tension is simply calculated from a nonlinear, static model based on the measured looper angle. The following sections deal with design and analysis of these control loops.

### 4.2.1 Design of looper position controller

Conventional looper position controller is a PI regulator indirectly affecting the looper angle by adjusting the loop length. The very nature of this control method and the fact that the PI controller is expected to function mainly in low frequency range suggest that the problem may be reduced to simple loop length regulation for the purposes of PI controller design. This is equivalent to neglecting the looper dynamics. Indeed it does not make much sense to consider looper dynamics while tension is controlled independently because the inertial torque of the looper is a strong disturbance to tension but has only a negligible effect on position. This reduction leads to the following simple model:

$$\frac{\Delta\theta(s)}{\Delta\omega_{ref}(s)} = \frac{k}{s(T_{md}s + 1)} \tag{4.4}$$

In Equation 4.4 the constant $k$ is equal to $d\theta/dL\ R_0(1 + \bar{f})$; the lag represents the main drive dynamics and the integrator converts speed into length.

The looper-strip system is theoretically stable. The pole-zero map of Looper 6 is shown in Figure 4.4 as an example. In the same plot, poles of the simple model in Equation 4.4 are also shown. It is seen that the pole close to origin has shifted to origin for the simplified case, making the process integrating. This is because the slip change due to tension variation is not accounted for in the latter, which should be better since tension is actually regulated. The two distant poles have also disappeared but their effect is mainly at high frequencies where the controller is not expected to be effective.
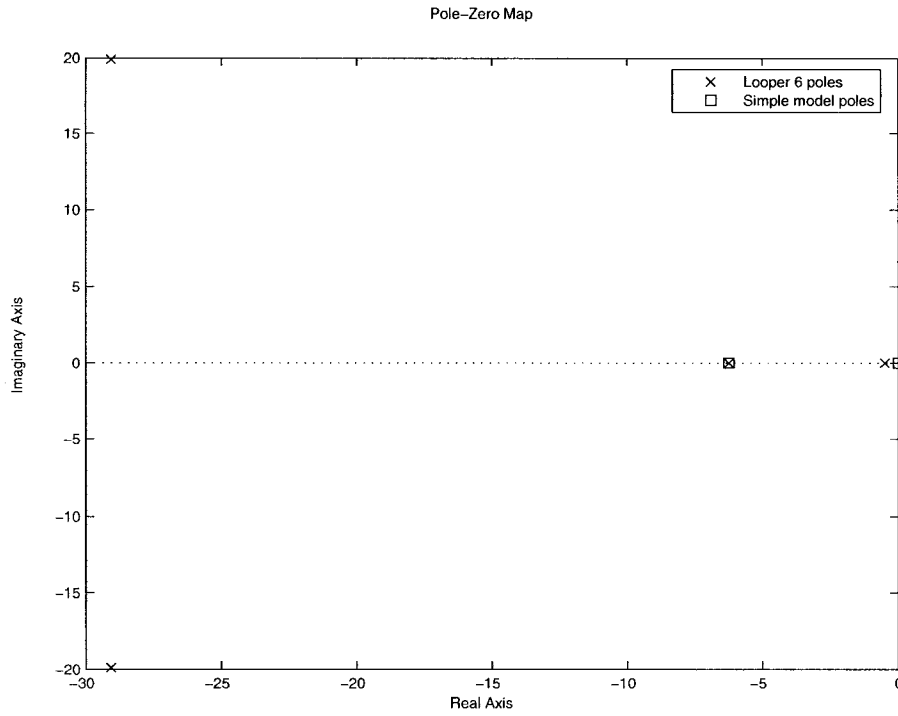
Figure 4.4: Pole-zero maps of original and simplified models for Looper 6

The controller tuning method preferred here is that of Wang and Cluett for integrating processes [34]. Tuning is based on selection of the parameters $\beta$ and $\zeta$ for shaping the desired controller response, which is expressed as:

$$G_{ru}(s) = \frac{s}{K} \frac{(2\zeta\tau + \gamma_1)s + 1}{\tau^2 s^2 + 2\zeta\tau s + 1} \qquad (4.5)$$

The natural period $\tau$ of the desired controller signal is selected as $\tau = \beta\gamma_1$ where $\gamma_1$ is the second coefficient of the Taylor series expansion of the integrating process $G_I$ around $s = 0$:

$$G_I(s) = \frac{K}{s}(1 + \gamma_1 s + \cdots) \qquad (4.6)$$

Thus, $\beta$ can be used to adjust the speed of the control signal. For lag dominant processes, which is defined as $\gamma_1 < 0$, it is recommended the damping factor $\zeta$ be selected as either $1/\sqrt{2}$ or 1. Then, the PID controller is found by dividing the desired open-loop transfer function $G_{ol}(s)$ by process transfer function $G_I(s)$ and fitting the result to a PID controller

form in the frequency domain. This procedure can be summarized as follows:

$$G_{ol}(s) = \frac{G_{ru}(s)G_I(s)}{1 - G_{ru}(s)G_I(s)} \tag{4.7}$$

$$c_2(j\omega)^2 + c_1(j\omega) + c_0 \approx \frac{G_{ol}(j\omega) \times j\omega}{G_I(j\omega)} \tag{4.8}$$

The two frequencies $\omega_1$ and $\omega_2$ necessary to calculate the constants $c_0, c_1, c_2$ in Equation 4.8 are selected as $2\pi/T_s$ and $4\pi/T_s$, $T_s$ being the desired closed-loop process output settling time. PID controller gain, and integral and derivative time constants are then simply $K_c = c_1$, $\tau_I = c_1/c_0$ and $\tau_D = c_2/c_1$, respectively.
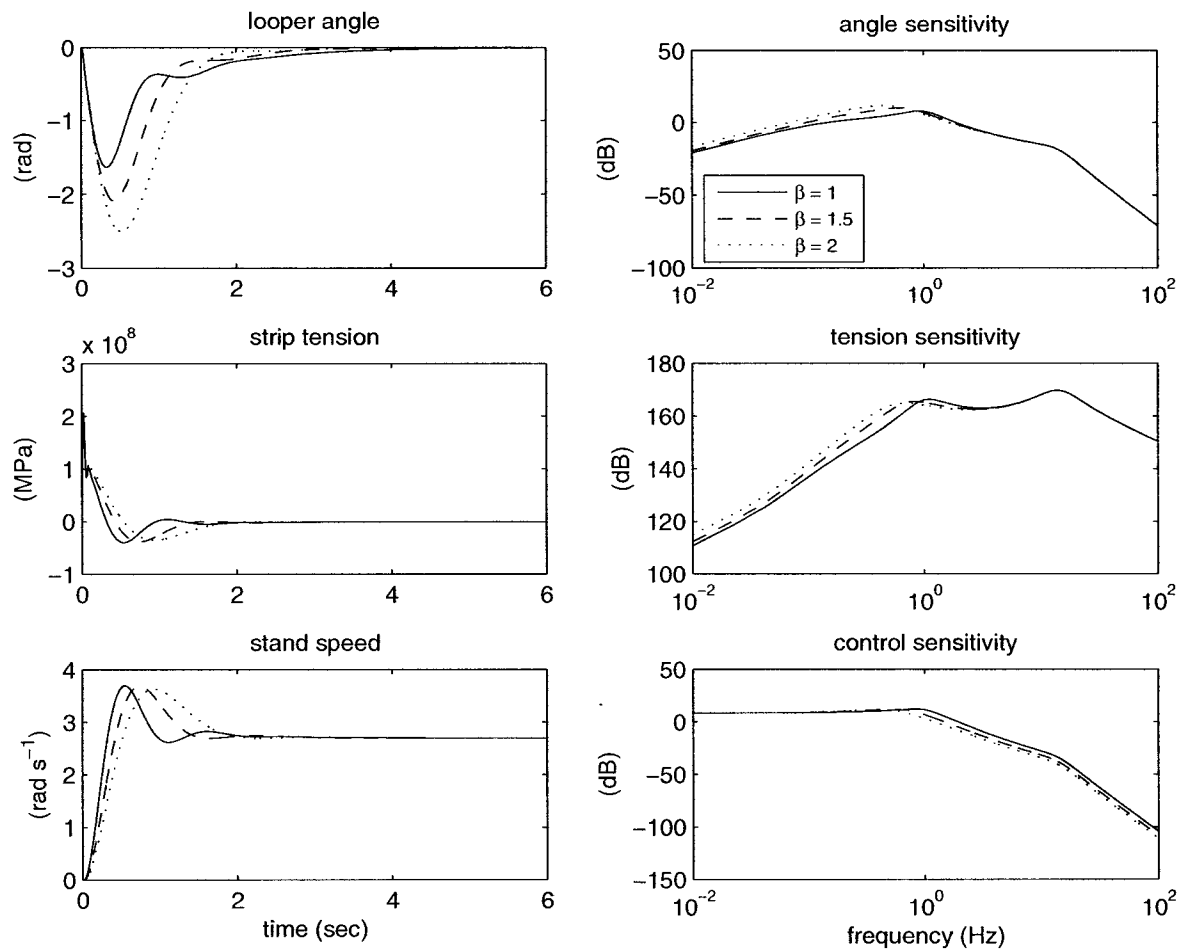


Figure 4.5: PI control disturbance rejection performance for Looper 1 ($\zeta = 0.707$)

It is clear from the analysis so far that dynamics of the main drive is the primary limiting factor when manipulating the looper. It does not make sense, therefore, to have a faster

controller than the main drive. In this particular case, values of the plant time constant and natural period of the controller are equal for $\beta = 1$. For higher values of $\beta$, the controller becomes slower following the rule $\tau = \beta\gamma_1$, as explained above. Looper 1 step disturbance rejection performance and closed loop sensitivities are presented in Figure 4.5 for $\zeta = 0.707$ and different values of $\beta$. $\zeta = 1$ also produces similar results.
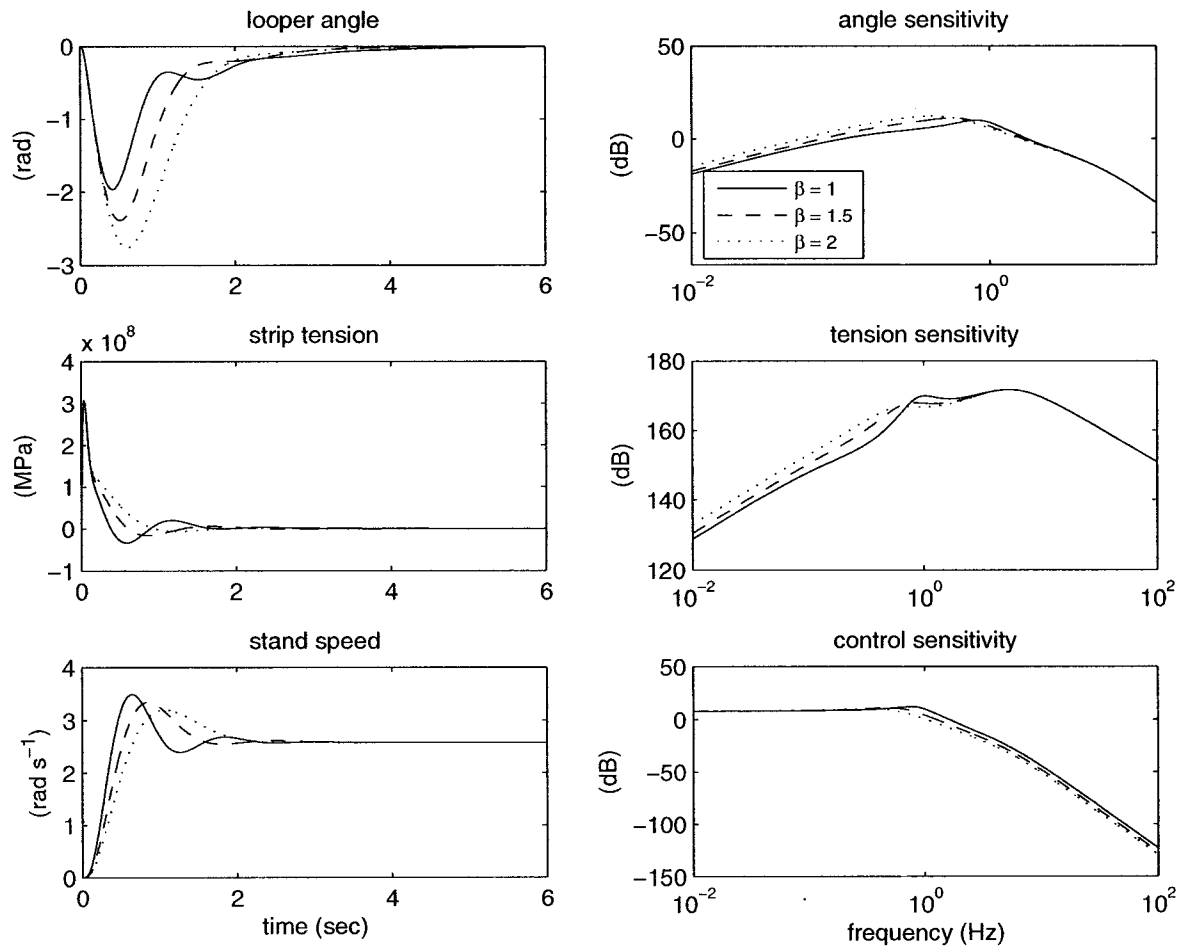


Figure 4.6: PI control disturbance rejection performance for Looper 6 ($\zeta = 0.707$)

A comparison of closed loop angle and tension sensitivities in Figure 4.5 to the open loop sensitivities in Figure 4.1 reveals that the PI controller is effective in controlling the looper angle as well as the strip tension mainly in low frequency range. Control signal sensitivity and output sensitivities clearly show that there is little control action above 1 Hz. The general observation from Figure 4.5 concerning the performance is that as the

controller becomes slower, performance deteriorates. Tension sensitivity plot suggests, however, slower controllers may have the edge for disturbances around 1-2 Hz, although they cause the angle to oscillate more. The trends are very similar for Looper 6 as seen in Figure 4.6.

## 4.2.2   Design of tension controller

Conventional tension controller is a nonlinear-static feedback system that adjusts the looper torque reference $M_{ref}$ to provide the reference tension $\sigma_{ref}$ utilizing the feedback looper angle $\theta$. The configuration is shown in Figure 1.3. Since it is a static controller, its output can be calculated off-line given the strip properties and reference tension. The output is plotted in Figure 4.7 for Loopers 1 and 6 for a range of $\mp 5°$ around the nominal angles of a typical rolling schedule.
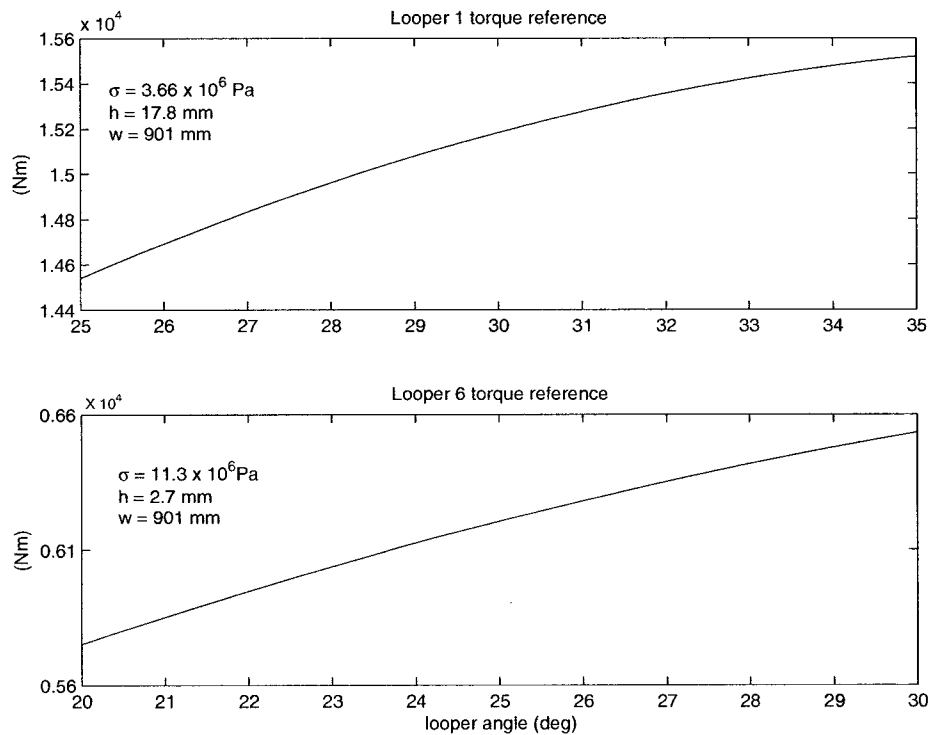


Figure 4.7: Tension controller output for Loopers 1 and 6

Looper load increases with increasing looper angle in Figure 4.7 because of the steeper strip angle which leads to a higher tension force. Although the output is not linear,

the controller may be approximated as a simple proportional feedback controller for the purposes of a linear investigation. The looper motor torque may then be expressed as:

$$\Delta M(s) = \frac{1}{\tau_F s + 1} \frac{1}{\tau_{cr} s + 1} \Delta M_{ref}(s) = \frac{1}{\tau_F s + 1} \frac{1}{\tau_{cr} s + 1} \frac{\partial M_L}{\partial \theta} \Delta \theta(s) \qquad (4.9)$$

where $\tau_{cr}$ is the current regulator time constant and $\tau_F$ is the filter time constant which is in the range $0.3 - 0.6$ sec. This filter is used in practice to prevent excessive response of the static controller in case of noisy feedback. The current regulator has a much wider bandwidth than the filter and its dynamics are negligible.
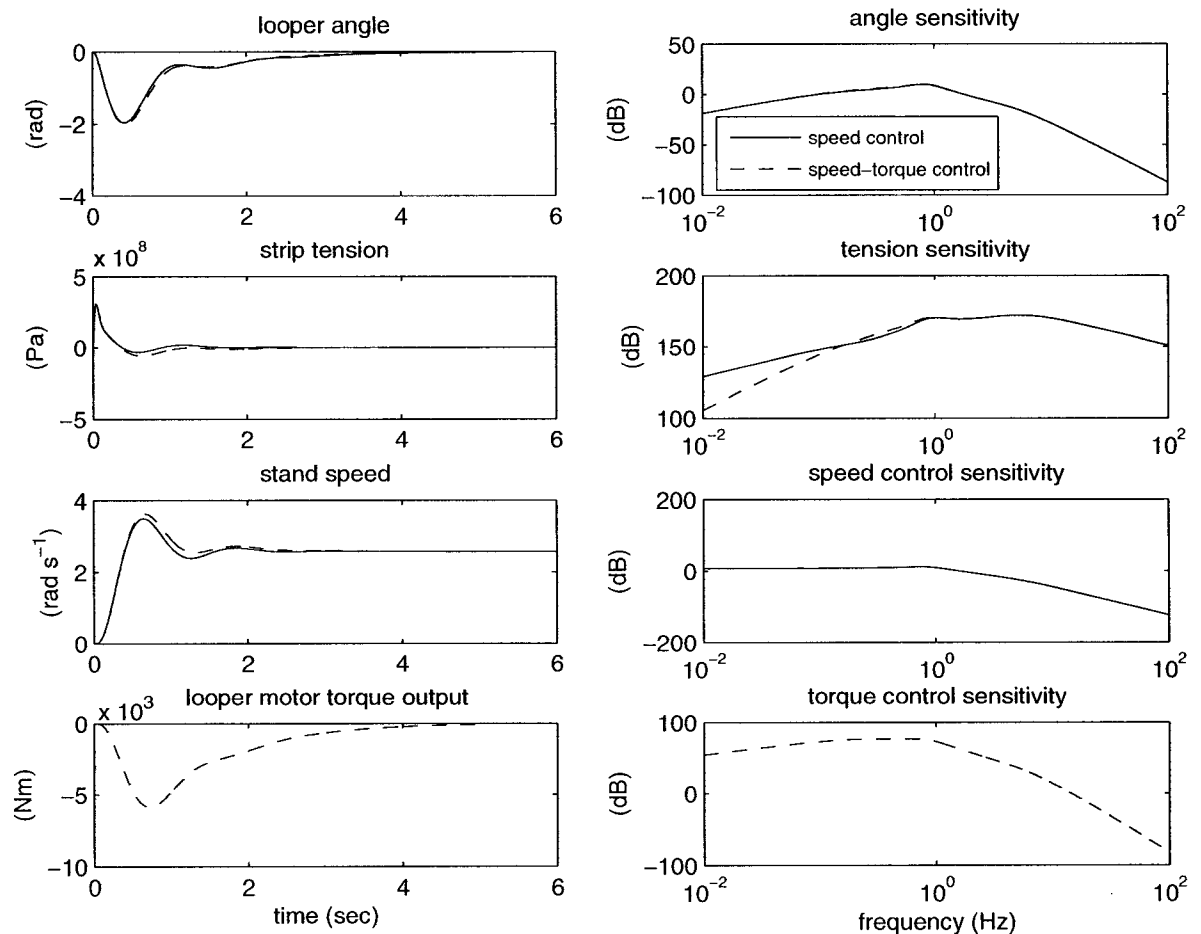


Figure 4.8: Tension controller contribution to Looper 6 performance ($\zeta = 0.707$, $\beta = 1$)

Performance improvement provided by the tension controller is shown in Figure 4.8 in the form of a comparison to the performance with speed controller only, which has previously been presented in Figure 4.6. The tension sensitivity plot indicates that the

performance is clearly better at frequencies below 0.2 Hz; whereas in the range 0.2-1 Hz the tension controller causes a discernible disadvantage. Its activity does not affect looper angle significantly, which is in agreement with the observation previously made in Section 4.1 that looper torque is not an input effective on looper angle.

# 4.3 Multivariable Control Design

A controller that combines the two independent loops discussed in Section 4.2 and uses looper angle feedback would be the simplest of multivariable looper controllers. The design could be improved via speed and tension feedback or by incorporating the gage control in the multivariable controller.

### 4.3.1 Controllability and observability analysis

The looper-strip system described in Equation 4.1 is controllable and can be observed using looper angle measurement, which is standard in hot strip mills. This form of the equations, however, cannot be used for optimal controller design because the resultant controller will not be able to remove the steady state errors. Time integrals of the controlled variables should also be controlled to prevent offset. This can be done using the following augmented system:

$$
\begin{bmatrix} \dot{x} \\ \dot{x}_6 \\ \dot{x}_7 \end{bmatrix} = \begin{bmatrix} A & \\ 1 & \\ 0 & 0 & 1 \end{bmatrix} \begin{bmatrix} x \\ x_6 \\ x_7 \end{bmatrix} + \begin{bmatrix} B_u \\ \\ \end{bmatrix} u + \begin{bmatrix} B_w \\ \\ \end{bmatrix} w \quad (4.10)
$$

$$
y = \begin{bmatrix} 1 & \\ 0 & 0 & 1 \\ & & 1 & 0 \\ & & & 1 \end{bmatrix} \begin{bmatrix} x \\ x_6 \\ x_7 \end{bmatrix} \quad (4.11)
$$

$$
(4.12)
$$

where vectors $x, u$ and $w$ correspond to the appropriate vectors of Equation 4.1 and states $x_6$ and $x_7$ are time integrals of angle and tension deviations, respectively. $y$ is the vector of controlled variables consisting of angle, tension and their accumulated deviations.

Although the system in Equation 4.10 solves the problem of steady state errors, it brings about a loss of observability. It is apparent that the additional states cannot be inferred from

an observation of looper angle because they have no influence on any of the physical states. This, however, does not pose a serious control problem. It is possible to design an observer with looper angle feedback via Equation 4.1, and produce the additional states $x_6$ and $x_7$ by integrating the measured angle and observed tension, respectively.

## 4.3.2 Looper covariance control problem

The multivariable controller design method applied here aims to produce a combined observer-state feedback system that guarantees covariance bounds on the controlled outputs while minimizing the control energy. The looper covariance control task may be described as designing a dynamic controller:

$$\dot{x}_c = A_c x_c + B_c z \tag{4.13}$$

$$u = C_c x_c \tag{4.14}$$

for the plant:

$$\dot{x} = Ax + B_u u + B_w w \tag{4.15}$$

$$y = C_y x \tag{4.16}$$

$$z = C_z x + v \tag{4.17}$$

so that the conditions:

$$\lim_{t \to \infty} E(yy^T) \leq Y \tag{4.18}$$

$$\lim_{t \to \infty} E(u^T R u) \leq \min \gamma \tag{4.19}$$

are satisfied. The plant in Equations 4.15 and 4.16 is the looper system given in Equations 4.10 and 4.11; $z$ here is the vector of measurements; $w$ and $v$ are white noises with intensity matrices $W$ and $V$, representing the speed disturbance and measurement noise. It is noted that matrix $Y$ in Equation 4.18 is simply an output covariance constraint and the scalar bound $\gamma$ is the minimal control energy satisfying the output covariance constraint.

Observability of the system in Equations 4.15 and 4.17 ensures that the controlled vector $y$ can be inferred from the vector of measurements $z$. It has been found that in order to make the system observable, $z$ must contain at least the accumulated angle and tension

deviations $x_6$ and $x_7$. As stated before, looper angle measurement is standard in hot mills and can easily be integrated. Tension is more often estimated than measured but in either case it can be integrated for controller use. Matrix $C_z$ of Equation 4.17 may then be written as:

$$C_z = \begin{bmatrix} & 1 & 0 \\ & & 1 \end{bmatrix} \tag{4.20}$$

An alternative to using the estimated tension may be using the dynamic portion of the controller as an observer and injecting the observed tension into the measurement vector after integration. On the other hand, using the plant tension estimate appears to be a better practice since it provides the controller with more information.

It is possible to solve the covariance control problem using linear matrix inequalities (LMIs). Feasibility of the controller in Equations 4.13 and 4.14 that stabilizes the plant and satisfies all design requirements can be related to the existence of some matrices satisfying specific LMIs [36]. The controller is parameterized using these matrices and can be easily computed, provided that they exist. This design method proposed by Zhang and Huang [36] ensures the global optimality of the controller.

## 4.3.3 Covariance control design

Solution of the covariance control problem stated in Equations 4.13-4.19 is only possible after specification of disturbance and noise intensities, output covariance and control input weighting. This leaves the designer with a large number of parameters. In such a case it will be convenient to decrease the number of design parameters by considering the variances only and leaving the cross elements of the covariance matrix $Y$ unspecified. Number of output covariance constraints to be specified is thus reduced from 10 to 4. The same approach can also be used for disturbance and noise intensity matrices.

Optimal controllers have large bandwidths and it is natural to expect that in this particular problem the control action will be focused around the resonance frequencies where the output sensitivities are the largest. It can be concluded from Section 4.1, however, that achieving control in this region may be very demanding or even impossible due to insensitivity to control inputs. Placing variance constraints directly on looper angle and strip tension would therefore be undesirable as this would carry the control action from low

frequency region to the resonance region. This suggests that it may be better to consider the integrated angle and tension errors only, and relax the angle and tension constraints to an extent that they will have no effect on the controller. In so doing, the number of output covariance constraints is further reduced to 2.

The strip speed disturbance $\Delta V$ in finishing mills is far from behaving like white noise. This follows the fact that major disturbances of a finishing mill have a cyclic nature often with a predictable spectral content. A quantitative inspection of plant disturbances can be found in Chapter 5. Proper modeling of these disturbances is not a straightforward task but simply filtering the high frequency content may still be useful to help focus on the low frequency range which includes the major disturbances and is sensitive to control inputs. With the augmentation of a first order, low-pass filter of bandwidth $\omega_F$, the looper covariance control problem attains the form shown in Figure 4.9. The measurement noise v will be assumed negligibly small in this study due to a lack of information about actual noise levels and measurement or estimation errors.
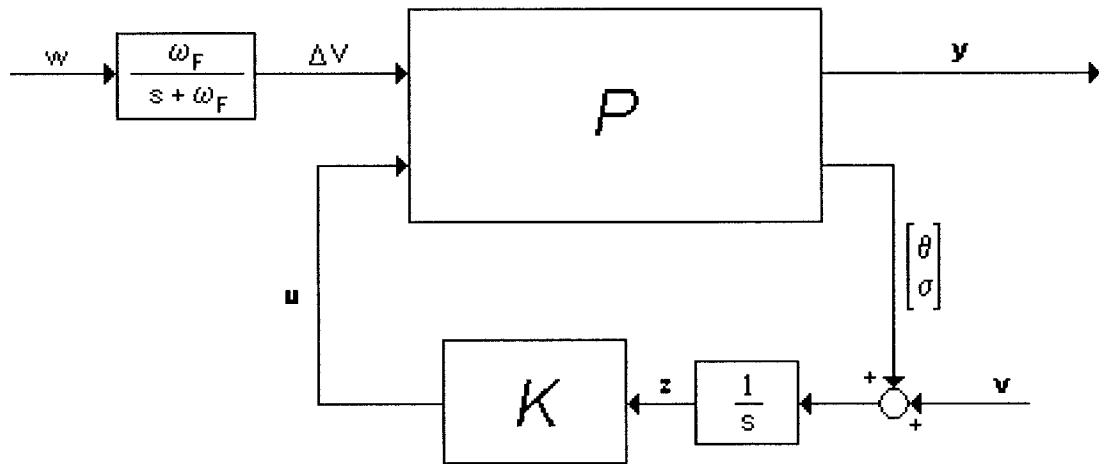


Figure 4.9: Block diagram for filter-augmented looper covariance control problem

Closed loop responses of covariance control for Looper 1 is shown in Figure 4.10 together with the benchmark conventional control performance. The design parameters used for controller design can be found in Table 4.1. Covariance controller 1 (C1-i) has been designed to emulate the PI controller. It is apparent that the covariance controller may be tuned to achieve substantially better regulation than the PI controller

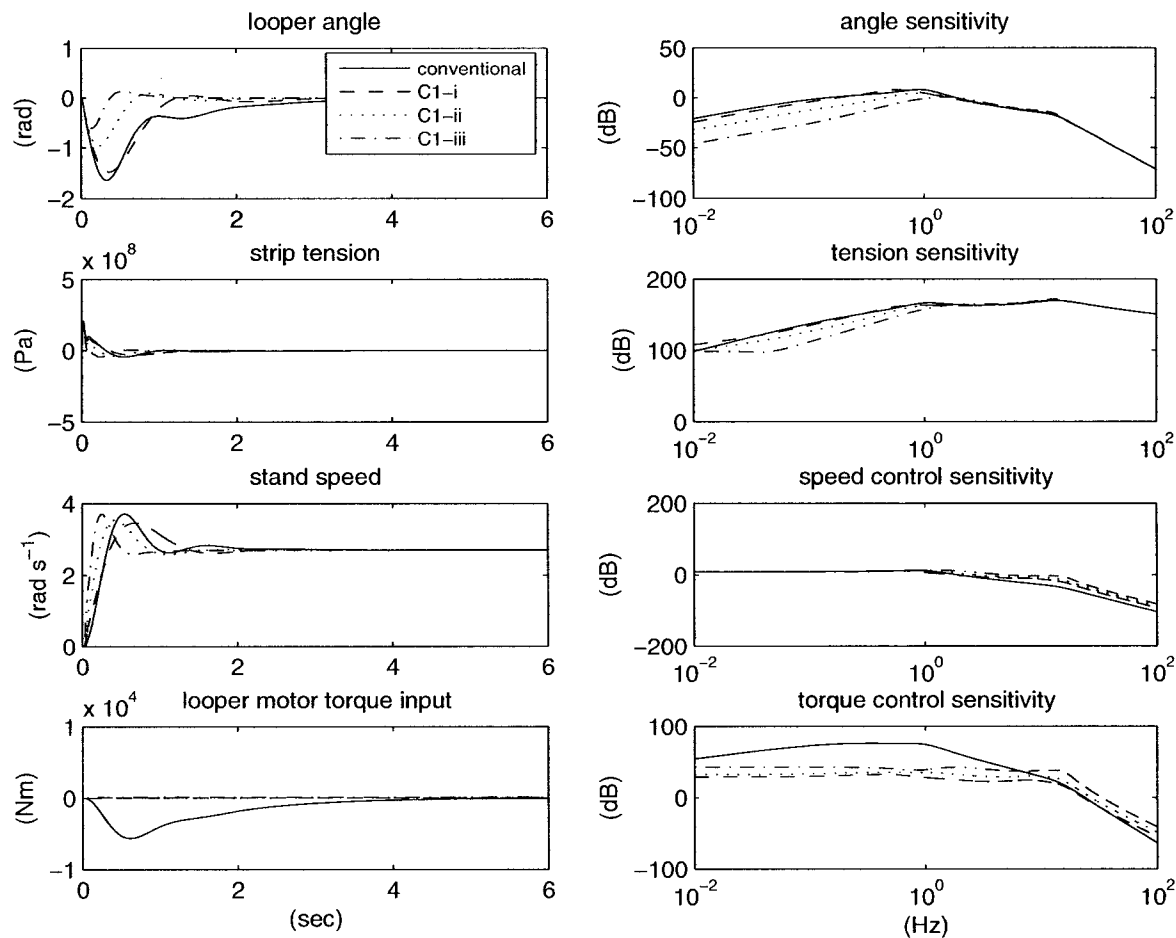| Controller | Design Parameters | | | | | | |
|---|---|---|---|---|---|---|---|
| | $\beta$ | $\zeta$ | var($\Delta V$) $(m^2s^{-2})$ | var($\int \theta dt$) $(rad^2)$ | var($\int \sigma dt$) $(Pa^2)$ | R | $\omega_F$ $(rads^{-1})$ |
| Conventional | 1 | 0.707 | | | | | |
| C1-i | | | $1 \times 10^{-9}$ | $10 \times 10^{-10}$ | $14 \times 10^6$ | I | 10 |
| C1-ii | | | $1 \times 10^{-9}$ | $2.5 \times 10^{-10}$ | $3.5 \times 10^6$ | I | 10 |
| C1-iii | | | $1 \times 10^{-9}$ | $0.5 \times 10^{-10}$ | $0.7 \times 10^6$ | I | 10 |

Table 4.1: Control design parameters for Looper 1



Figure 4.10: Covariance control disturbance rejection performance for Looper 1

in exchange for more speed control use. Speed control sensitivity naturally increases with increasing performance as seen in cases C1-ii and C1-iii and the durability and tracking ability of the main drive may become a limiting factor in looper control besides

the robustness considerations. A noteworthy observation from Figure 4.10 is that the multivariable controller's use of looper torque is negligible compared to that of the static tension regulator. Torque use may be favored by changing the input weight factor R, but this results in inferior control with high closed loop gains at low frequencies.
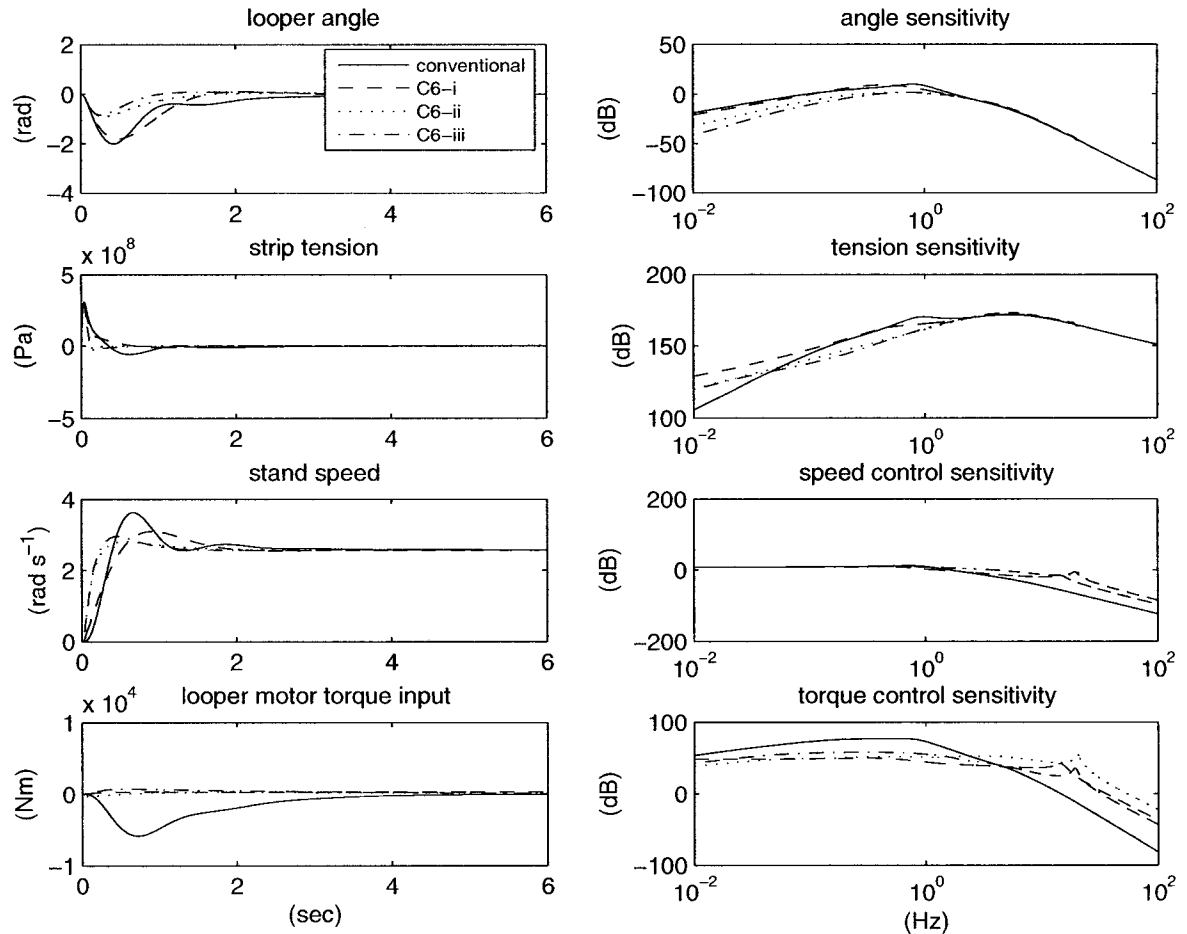


Figure 4.11: Covariance control disturbance rejection performance for Looper 6

Figure 4.11 shows the covariance control's closed loop responses for Looper 6. The trends appear to be very similar to those of Looper 1, with the notable exception of more torque use. It is also interesting that the covariance controller uses the torque in the opposite direction, which points out that in multivariable case the torque input is paired with the looper position rather than strip tension. This becomes more obvious when controllers C6-ii and C6-iii are compared. As seen in Table 4.2, the only difference between these controllers is the tighter variance bound on looper angle for C6-iii. In Figure 4.11 it can

be observed that C6-iii achieves this by using more torque only and that speed control essentially remains the same. Looper 6 has substantially thinner strip compared to Looper 1, which makes the torque a more effective input. Torque gains on looper position can be found in Figure 4.3 for Looper 1 and 6.

| Controller | Design Parameters | | | | | | |
|---|---|---|---|---|---|---|---|
| | $\beta$ | $\zeta$ | var($\Delta V$) (m$^2$s$^{-2}$) | var($\int \theta dt$) (rad$^2$) | var($\int \sigma dt$) (Pa$^2$) | R | $\omega_F$ (rads$^{-1}$) |
| Conventional | 1 | 0.707 | | | | | |
| C6-i | | | $1 \times 10^{-9}$ | $20 \times 10^{-10}$ | $28 \times 10^6$ | I | 10 |
| C6-ii | | | $1 \times 10^{-9}$ | $5 \times 10^{-10}$ | $1.4 \times 10^6$ | I | 10 |
| C6-iii | | | $1 \times 10^{-9}$ | $2.5 \times 10^{-10}$ | $1.4 \times 10^6$ | I | 10 |

Table 4.2: Control design parameters for Looper 6

## 4.4 Feedforward Control

As noted in Section 4.1, the direct disturbance on the looper system is the strip speed imbalance $V_{i+1} - v$, which is affected by stand speeds and a number of disturbances such as gage and temperature fluctuations or roll eccentricity. The control quality may therefore be significantly improved if the strip speeds can be predicted and utilized in feedforward mode.

The feedforward problem is to find the necessary speed correction amount $\Delta \omega^i_{ff}$ for Stand i to negate the effect of downstream strip entry speed change $\Delta V_{i+1}$ and the slip variation of the stand itself $\Delta f^i$. It should be possible to decouple the looper from the downstream looper and effect of the slip change by adding this amount to the controller output $\Delta \omega^i_{ref}$:

$$\Delta \omega^i_{REF} = \Delta \omega^i_{ref} + \Delta \omega^i_{ff} \tag{4.21}$$

Thus, the first term regulates the looper and the second term may be regarded as a decoupler. $\Delta \omega^i_{REF}$ in Equation 4.21 is the signal to the main drive speed regulator.

The necessary amount of speed correction $\Delta \omega^i_{ff}$ can be calculated starting with the fact that the strip exit speed $v$ and the downstream strip entry speed $V_{i+1}$ should ideally be equal

at all times, i.e.

$$\Delta v - \Delta V_{i+1} = 0 \tag{4.22}$$

An expression for strip entry speed can be obtained by linearizing Equation 2.50:

$$\Delta V = \frac{\bar{h}}{\bar{H}}\Delta v + \frac{\bar{v}}{\bar{H}}\Delta h - \frac{\bar{v}\bar{h}}{\bar{H}^2}\Delta H \tag{4.23}$$

Linearization of Equation 2.49 leads to the following relationship for the exit speed $\Delta v$:

$$\Delta v = R_0(1 + \bar{f})\Delta\omega + R_0\bar{\omega}\Delta f \tag{4.24}$$

Thus, it is possible to obtain an expression for $\Delta V_{i+1}$ by substituting Equation 4.24 into Equation 4.23. Equation 4.22 can then be expanded using this expression and Equation 4.24 for $\Delta v$ to yield the following relationship for the amount of speed correction:

$$\Delta\omega_{ff}^i = \alpha_\omega^{i+1}\Delta\omega^{i+1} + \alpha_f^{i+1}\Delta f^{i+1} + \alpha_h^{i+1}\Delta h^{i+1} + \alpha_H^{i+1}\Delta H^{i+1} + \alpha_f^i\Delta f^i \tag{4.25}$$

where $\alpha$'s are the proper groups of terms.

It is apparent from Equation 4.25 that full compensation is a complex task requiring information about gage and slip variations, none of which are measured. A first approximation to Equation 4.25 is to preserve the first term only since it is relatively independent of the others and does not require unavailable measurements:

$$\Delta\omega_{ff}^i = \alpha_\omega^{i+1}\Delta\omega_{ref}^{i+1} = \frac{\bar{h}^{i+1}}{\bar{H}^{i+1}}\frac{R_0^{i+1}}{R_0^i}\frac{(1 + \bar{f}^{i+1})}{(1 + \bar{f}^i)}\Delta\omega_{ref}^{i+1} \tag{4.26}$$

The stand speed term $\Delta\omega^{i+1}$ in Equation 4.25 is replaced with stand speed reference $\Delta\omega_{ref}^{i+1}$ in Equation 4.26 to allow the speed regulator of Stand i more time to adapt. This form of the feedforward is used in conventional control systems to decrease the working range of the loopers. Simulations have shown that conventional control system would otherwise have stability problems. The feedforward signal can be located in the conventional control arrangement presented in Figure 1.3, where the gain *nominal speed ratio* corresponds to $\alpha_\omega^{i+1}$.

Further attempts in feedforward control must involve estimation of gage and slip variations. Slip variation is in fact mainly a function of gage variations. Thus, the other dependencies may be neglected and Equation 2.48 may be linearized to yield:

$$\Delta f = \frac{\partial f}{\partial h}\Delta h + \frac{\partial f}{\partial H}\Delta H \tag{4.27}$$

Using Equation 4.27, $\Delta f^i$ and $\Delta f^{i+1}$ in Equation 4.25 can be expanded in terms of gage variations. With a regrouping of terms, Equation 4.25 becomes:

$$\Delta \omega^i_{ff} = \alpha^{i+1}_\omega \Delta \omega^{i+1} + \beta^{i+1}_h \Delta h^{i+1} + \beta^{i+1}_H \Delta H^{i+1} + \beta^i_h \Delta h^i + \beta^i_H \Delta H^i \qquad (4.28)$$

Hence the problem is reduced to estimating the entry and exit gage variations for both stands. Among these, exit gages may be inferred using the force measurements and Equation 2.27:

$$\Delta h = \Delta C_{ref} + \frac{\Delta F}{K_s} \qquad (4.29)$$

Again, the position reference to the actuator is used instead of the actual position to provide more time for the speed regulator.

Estimation of entry gage is a more complex task. Entry gage variation $\Delta H^{i+1}$ is in fact the delayed exit gage variation $\Delta h^i$ from the upstream stand but the fact that the delay is varying complicates the matters. Rigler et al. [26] and Keintzel et al. [19] describe use of a Kalman filter and strip segment tracking algorithm to infer the gage variations and handle the transport delay. This sophisticated system operates with buffers similar to the one described in Section 2.6 to store the values before they reach the downstream stand. Hence, at least in plants equipped with this kind of estimator, it is possible to fully use Equation 4.28 for feedforward.

*"Mr Churchill is easily satisfied with the best."*
— Lord Birkenhead

# 5

# Model and Control Performance

As the discussions heretofore should have made clear, the finishing mill is a complex plant with strong interactions between its units and is equipped with many control loops. A lack of open loop data, unknown controller structures and tuning, and scarce measurements render model validation and calibration difficult. In such a case it makes more sense to consider the plant and controller models together and expect their performance to match the real plant performance at some reasonable calibration and controller tuning.

This chapter starts with evaluating the model performance through simulation of rolling of a real coil. Rest of the chapter deals with assessment of the controllers designed in Chapter 4 based on the evaluated model.

## 5.1 Model Performance

In general, it is desirable to use open loop plant data for model validation studies but absence of such data and the difficulty of running a finishing mill without control necessitate other approaches to be devised.

The model performance can be assessed by simulating rolling of a real coil and comparing the simulation outputs to the plant data for this particular coil. Simulation

60

of a real rolling process requires knowledge of the main disturbances such as mill entry temperature, mill entry gage and roll eccentricity, as well as knowledge of the plant control arrangements and tuning. The facts that not all disturbances are measured in a finishing mill and there is a considerable lack of information about the plant controllers are the main difficulties with this approach.

Although there is no direct information regarding the disturbances such as mill entry gage or roll eccentricities, these may be inferred from their effect on looper behavior or other available plant data. Thus, through an iterative process involving the simulator, it may be possible to obtain some estimates of these disturbances. Since little is known about plant control structure and tuning, the simulator's control systems have to be designed in a representative manner. The tuning can be changed within reasonable limits to provide better agreement between the simulator outputs and plant data. It is inevitable during the process described above to incur some errors due to the interactions between the process outputs, disturbances, and plant control systems; however, an approximation of the model performance may still be obtained.

The next section deals with the estimation of the disturbances. A brief description of plant control systems and tuning is given in the section following it, before attempting the performance assessment task.

## 5.1.1 Disturbance estimation

Mill entry temperature and gage, roll eccentricities and mill entry tension shock caused by the crop shear are the disturbances considered in this section.

In a finishing mill, strip entry temperature is generally measured by pyrometers some distance ahead of the first stand. The temperature measurements recorded before onset of threading is not useful because they cannot be converted to a length base due to unknown timing and duration of descaling. This confines the comparison to the second minute of the operation. Assuming the radiation loss and spray cooling do not change the frequency content and relative magnitudes of the signal significantly, the mill inlet temperature may be replaced with the measured profile provided that it is corrected for the distortion created by mill acceleration. The corrected profile is shown in Figure 5.1 together with its frequency

content. The period of last 10 seconds is an artificial extension to cover the time elapsed before the tail end leaves Stand 7. The constant decrease in temperature is due to the longer period of radiation loss experienced by the tail end.
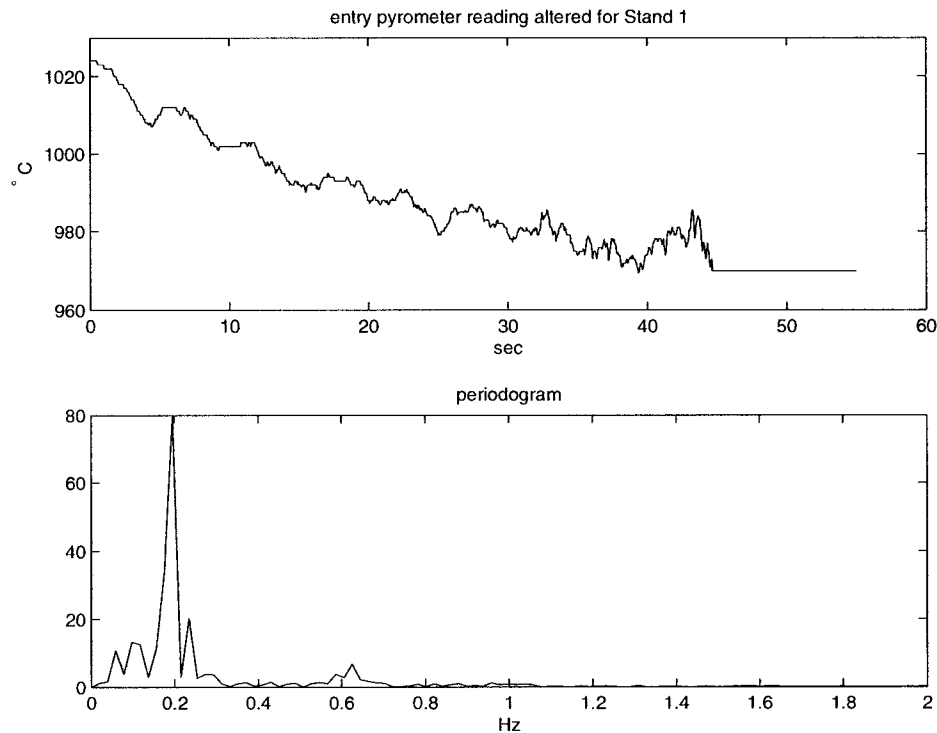


Figure 5.1: Inlet pyrometer reading modified for Stand 1 entry and its periodogram

The entry gage is typically not measured. Fortunately, entry gage is a less significant disturbance than the entry temperature because it is corrected at each stand by stand gage controllers. Thus, its effect on stand behavior is likely to fade away as the stand number increases. It may be possible to obtain some information about the entry gage by using the exit gage from Stand 1, which is estimated from Equation 2.27, the gage-meter equation. In this particular case, the entry gage is likely to be a sinusoidal with an amplitude of 0.5 mm and frequency ranging from 0.22 Hz to 0.38 Hz, probably due to mill acceleration.

It is difficult to obtain magnitude and phase data for eccentricity of the rolls during a specific operation. Further, depending on the gage control method used by a particular stand, the same amount of misalignment may have substantially different effects on looper motion. Considering the lack of information about the misalignments and gage controllers,

it is convenient to calibrate the eccentricities so that their effects on loopers are at a similar level to those of the real eccentricities. By altering Equation 2.27, roll eccentricity may be simulated as a sinusoidal disturbance on the loaded roll gap:

$$h = C + \frac{F}{K_s} + e_w \sin\{\omega(t)t\} + e_b \sin\{\omega_b(t)t\} \tag{5.1}$$

where $\omega(t)$, $\omega_b(t)$ are work roll and backup roll rotation frequencies; and $e_w$, $e_b$ are respective eccentricity magnitudes. $0.3 - 4$ Hz is a typical frequency range for backup rolls of a finishing mill. Major effects are generally due to backup rolls which are maintained less often. Nonetheless, work rolls can also cause significant disturbances owing to their high frequency of rotation, approximately twice of the backup rolls.

The crop shear, when functioning, slightly decreases the strip velocity at the cutting point, which is some distance ahead of the first stand. This disturbance should cause an abrupt increase in entry tension, whose effect is obvious from the large deviation in Looper 1 angle. The magnitude profile and duration of this tension shock are unknown but it has been possible to create a similar effect on Looper 1 by assuming a profile and modifying it as necessary.

Having thus estimated some major disturbances, it may be useful to inspect the spectral densities of the mill outputs, which are given and discussed in more detail in §5.1.3 . An interesting situation arises when the predominant excitation frequency of each looper is checked: Loopers 2, 5 and 6 exhibit peaks mainly at 0.2 Hz, while Loopers 1, 3 and 4 do so at 0.3 Hz. Considering that the mill entry temperature has a peak around 0.2 Hz as seen in Figure 5.1, the looper motion at this frequency may be expected; however, none of the disturbances discussed thus far is likely to cause excitations around 0.3 Hz. The fact that Loopers 3 and 4, which are both adjacent to Stand 4, are strongly affected by this disturbance implies the possibility that Stand 4 hydraulic gage control system, the first hydraulic system in line, receives and amplifies some small disturbance around 0.3 Hz. In fact, simulations have shown that a sinusoidal force disturbance with an amplitude of less than 1 % of the nominal stand force value can cause such a severe effect in simple force feedback case. This kind of a force fluctuation might have been caused by a flatness defect in the strip.

The question of how Stand 2 data have no content at 0.3 Hz, however, still remains. It

would be expected that due to Stand 3 controller responding to Looper 3 angle feedback at 0.3 Hz, Looper 2 should also be affected, especially in absence of speed feedforward between the stands. An explanation could be that Stand 2 also received some disturbance at 0.3 Hz, thus negating the effect of the downstream disturbance. The hypothesis of counterbalanced disturbances also explains well the excitation of Looper 1 at that frequency. While negating the effect of the downstream speed fluctuations for Stand 2, such a disturbance would naturally disturb Looper 1. Simulations have shown that very realistic results are obtained if these speculations are assumed true.

## 5.1.2   Simulator control systems

Information regarding the actual controller structures and tuning, especially those of the gage controllers, may be crucial for the successful simulation of a real rolling process. Since there is a considerable lack of information about the plant control systems and some of these systems have not been modeled, here it may be better to set up the simulator in a representative manner rather than attempting to produce the real setting that was in operation. As stated before, relatively less significant systems such as shape or temperature control are omitted in this study and only the looper and gage control are considered. Among these, the looper control have already been discussed in detail and the simulator's gage control setup is explained below.

First three stands of the simulator are equipped with electromechanical screws as roll actuators while the rest have hydraulic actuators. Mill stretch is compensated at all stands except Stands 2 and 3 via simple force feedback loops. These loops are tuned to provide less than full compensation, as it is generally the case in practice due to the uncertainty in stand stiffness $K_s$. A final gage control loop that uses the mill exit gage measurement in feedback mode is also installed on Stand 7. Fine tuning of these controllers as well as the looper controllers have been carried out so that the simulation results are closer to reality.

## 5.1.3   Model performance assessment

The plant data and simulation results for Loopers 1 and 2 are shown in Figure 5.2. The excitation of Looper 1 at 0.3 Hz is assumed to be caused by a flatness defect affecting

Stand 2, which is simulated as a sinusoidal disturbance on Stand 2 exit gage. It should be noted that proper simulation of a flatness disturbance requires a two dimensional model and the method used here can only be approximate. The big deviations in angle and tension at around $t = 95$ sec is caused by the crop shear that is located before Stand 1 and cuts the tail end of the strip. A similar disturbance has been created in the simulation by introducing an inlet tension shock whose size and timing are adjusted so that the impact on the looper is at a realistic level. Finally, the small fluctuations in the range $0.35 - 0.8$ Hz are due to Stand 1 and 2 backup roll eccentricities. Results suggest that the model captures the main dynamics of the process. It is remarked here that the plant tension data is not a measurement but an estimate and so caution should be applied when using it as a means of assessment of the model performance.
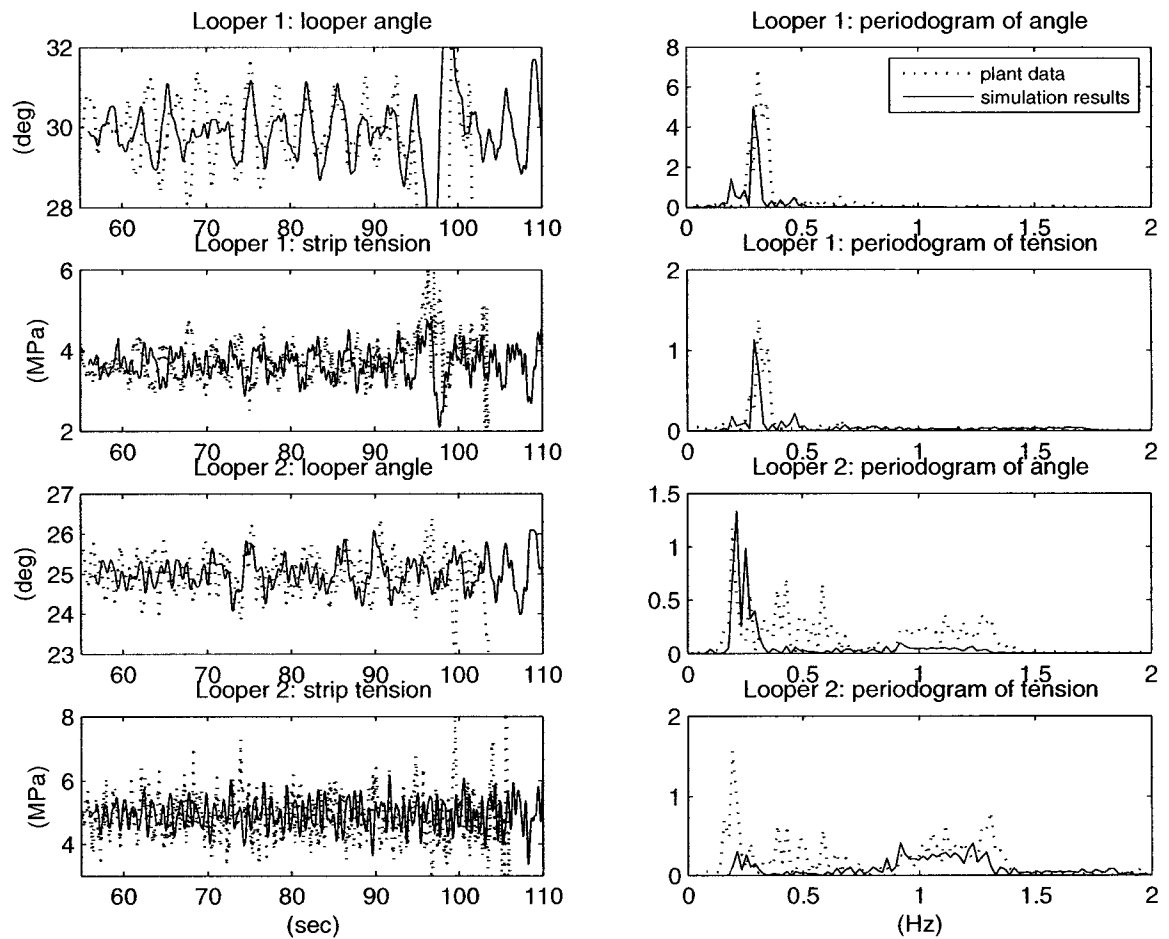
Figure 5.2: A comparison of plant data and simulation results for Loopers 1 and 2

It is seen in Figure 5.2 that Looper 2 motion is dominated at around 0.2 Hz by the mill entry temperature and in the range 0.9-1.4 Hz by Stand 3 backup roll eccentricity. The flatness defect that is assumed to exist and disturb Stand 2 has no visible effect here because it is counterbalanced by the downstream disturbance at 0.3 Hz originating from Stand 4. The fluctuations in the range 0.4-0.6 Hz in plant data could be because of Stand 1 backup roll eccentricity or Stand 2 gage controller strongly responding to the entry temperature fluctuation at 0.6 Hz seen in Figure 5.1. Since the structure of the gage controller is not exactly known, a more definitive statement cannot be made. The differences in tension could be due to an estimation error in the plant data or different controller tuning or structure.
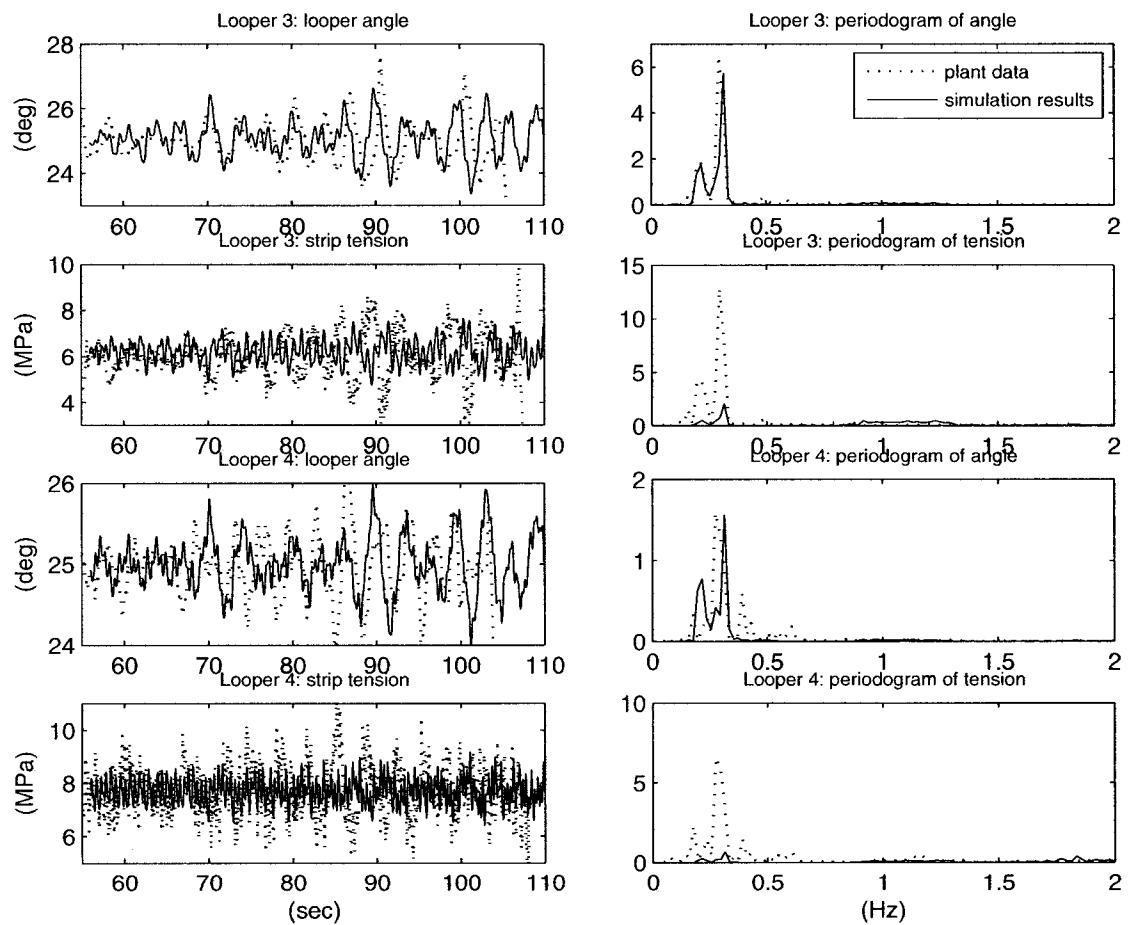
Figure 5.3: A comparison of plant data and simulation results for Loopers 3 and 4

Figure 5.3 indicates that both Loopers 3 and 4 are predominantly excited at 0.3 Hz.

In Section 5.1.1 it has been proposed that this excitation might be because Stand 4 gage controller amplifies some small disturbance produced by a flatness defect in the strip. Simulation results here shows that this is indeed a possible cause.
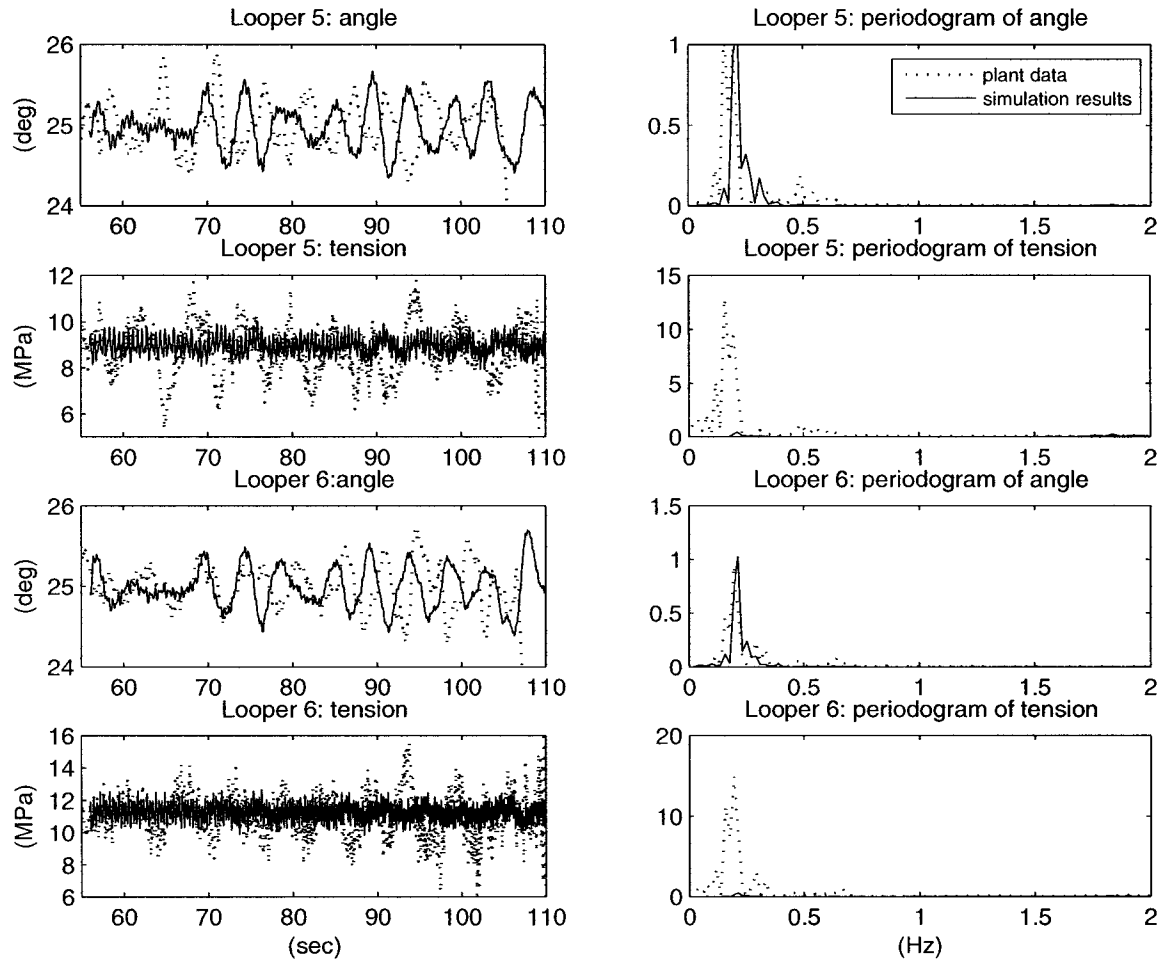


Figure 5.4: A comparison of plant data and simulation results for Loopers 5 and 6

The plant data and simulation results for Loopers 5 and 6 are plotted in Figure 5.4. Although there is a phase difference, the actual and simulated angle profiles are similar. It has been found that the phase shift may be a result of different gage or looper control tuning. On the other hand, the reason for the substantial difference in tension predictions is not very clear. The tension is estimated based on looper motion and an agreement would be expected as long as the looper motion is predicted accurately. Now it may only be speculated that the plant controllers use the torque input in a significantly different way

than the simulator controllers do, or the plant tension estimation is not very accurate.

The errors in simulator predictions may be due to a number of reasons such as different plant and simulator control systems and tuning, disturbance estimation errors, unknown disturbances and the phenomena that are not modeled. It should be remembered that the only piece of dynamic data taken from the real operation is the entry temperature profile. In spite of these limitations, the simulator outputs are quite realistic for a majority of cases. The model grasps the main dynamics of the finishing mill adequately and is also able to accurately handle a difficult problem such as the variable inter-stand transport delays. At this point it can be concluded that the model can find useful applications in both looper control design and control performance assessment.

## 5.2   Control Performance

Finishing mill control performance should be assessed not only in terms of disturbance rejection but also in terms of input use since the results of §4.3.3 suggest that part of a multivariable controller's superiority may come from excessive control energy use. At this point it appears to be a good practice to take the conventional control performance as a benchmark to assess the improvements in disturbance rejection as well as the input use. Signal variance could be a good quantitative performance indicator for a regulation task such as this.

The disturbances that will be used to test the controllers are similar to the estimated disturbances described in §5.1.1. The mill entry temperature, roll eccentricities and mill entry gage remain the same; the flatness defect that is assumed to disturb Stand 4 is increased in effect and the counterbalancing flatness disturbance at Stand 2 is omitted to enhance the impact of the first disturbance and help the comparison.

In practice it is not likely to find a conventional hot mill control system operating without speed feedforward action, but in some cases the multivariable controllers may function without it. In the following section, however, both conventional and multivariable controllers are evaluated in absence of feedforward so that a proper comparison can be made; in the next section improvements brought in by the feedforward action are presented.

## 5.2.1 Conventional and multivariable control performance

In §4.2.1 it has been concluded that conventional controllers with faster responses achieve better control except for an insignificant disadvantage they cause in tension sensitivity in the range 1-2 Hz. It therefore makes sense to choose $\beta = 1$ for design of the benchmark conventional controllers, which makes the natural period of the controller response equal to time constant of the actuator. In practice, such aggressive controllers are unlikely to be employed due to stability problems but robustness considerations are beyond the scope of this study. The design parameters used for the covariance controllers can be found in Table 5.1 in form of a comparison to controller C1-i of Chapter 4; the factor $\kappa$ indicates what fraction of C1-i output covariance constraint matrix is used for a particular controller, other design parameters remaining the same. The design parameters for C1-i can be found in Table 4.1.

| Looper number | Design Parameters | | Signal Variances | | | |
|---|---|---|---|---|---|---|
| | $\beta$ | $\kappa$ | $\theta \times 10^5$ | $\sigma \times 10^{-11}$ | $\omega_{ref} \times 10^4$ | $M_{ref} \times 10^{-3}$ |
| 1 | 1 | | 26 | 1.6 | 18 | 6.2 |
| | | 0.5 | 3.6 | 0.68 | 4.5 | 0 |
| 2 | 1 | | 86 | 9.5 | 34 | 34 |
| | | 0.45 | 7.8 | 2.5 | 8.5 | 0 |
| 3 | 1 | | 130 | 14 | 44 | 35 |
| | | 0.3 | 8.4 | 2.9 | 12 | 0 |
| 4 | 1 | | 97 | 12 | 35 | 21 |
| | | 0.27 | 4.4 | 2.8 | 6.9 | 0 |
| 5 | 1 | | 66 | 8.5 | 27 | 10 |
| | | 0.27 | 1.6 | 1.7 | 3.6 | 0 |
| 6 | 1 | | 25 | 5.4 | 11 | 4 |
| | | 0.33 | 0.75 | 2.9 | 1.9 | 0 |

Table 5.1: Output and input variances under conventional and covariance control in absence of feedforward

Variations of looper angle and strip tension with time under conventional and covariance controllers are given in Figure 5.5. Variance information for these signals and control inputs are provided in Table 5.1 The results show that the conventional controllers have a clearly inferior performance in spite of the large amount of control energy they consume. It is also observed that looper angle deviations enlarge with time under these controllers,

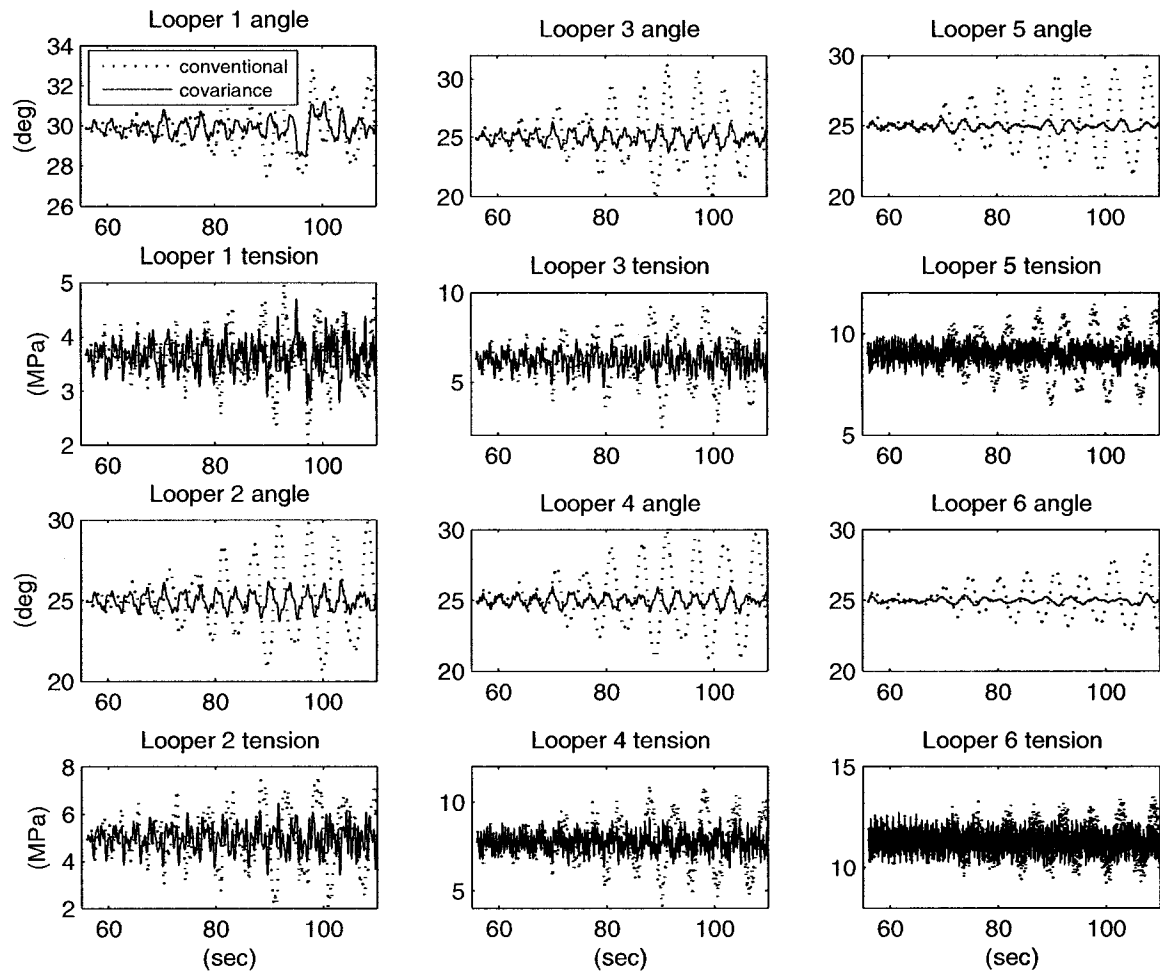which is likely to be a consequence of the mill acceleration leading to higher disturbance frequencies.



Figure 5.5: Conventional and covariance control performance in absence of feedforward

## 5.2.2 Contributions of the speed feedforward

Simulations have shown that even in its simplest form described by Equation 4.26, the speed feedforward brings in drastic improvements in terms of both disturbance rejection capability and reduction of control energy. Simulation results with feedforward mode on are shown in Figure 5.6. It is emphasized here that the same controllers described in §5.2.1 are employed in this simulation and the only difference is the speed feedforward action. Variance information for the output signals and control inputs are provided in Table 5.2.
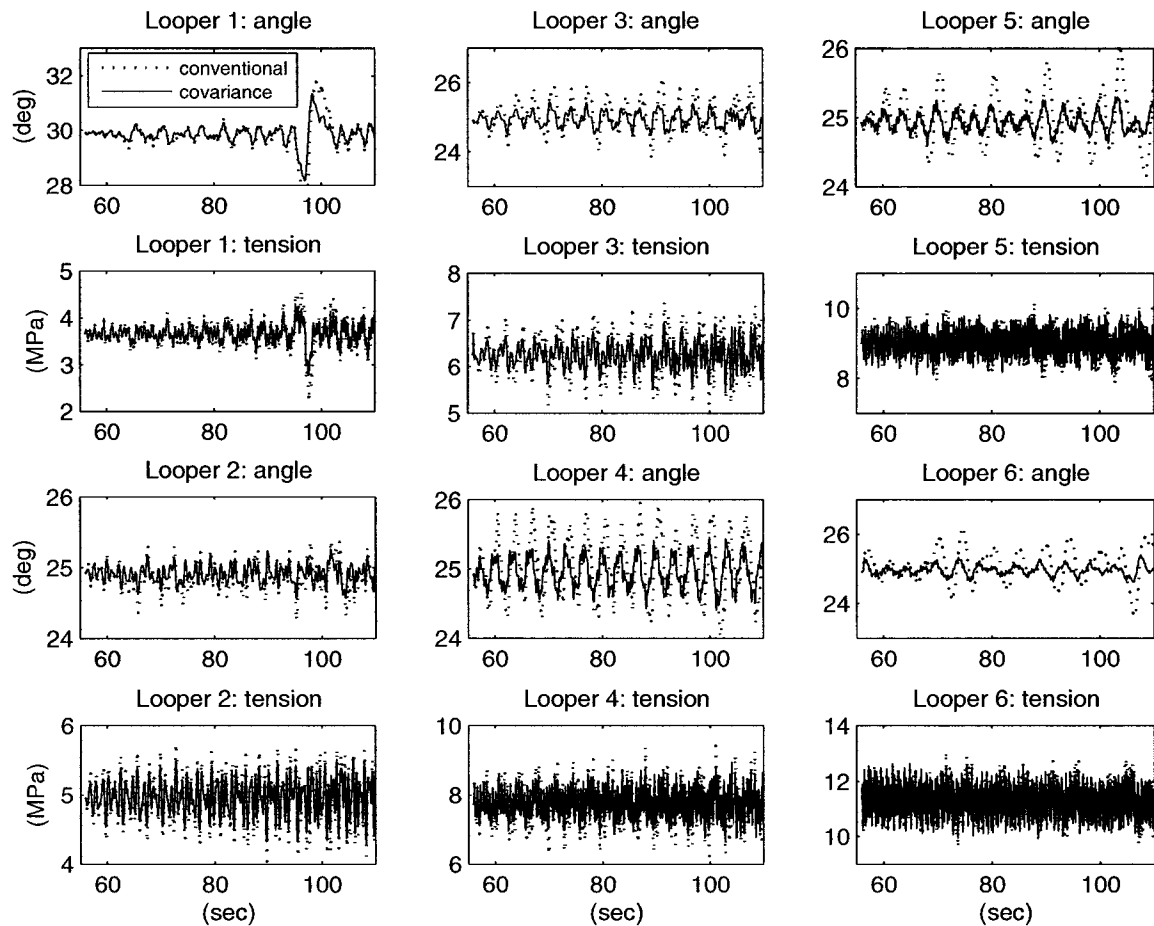
Figure 5.6: Conventional and covariance control performance with feedforward

The results also show that with speed feedforward, the conventional controller can close the gap with the multivariable controller for the earlier stands; however, in the case of later stands, the multivariable controllers are superior. This agrees with the conclusion made in Section 4.1 that it is more difficult to control the later loopers. Another notable fact is that the covariance controller achieves its better performance by using less input energy; Table 5.2 indicates that its use of torque is almost negligible and its use of speed is in most cases less than that of the conventional controller. The stand speed reference signals produced by conventional and covariance controllers are given in Figure 5.7 in deviational form together with the variations in the main drive motor's torque, which tries to accommodate these changes. The linear trend in speed reference signal is due to stand exit gage, which slightly increases in time because of diminishing temperature and reduced the amount of slip.

| Looper number | Design Parameters | | Signal Variances | | | |
|---|---|---|---|---|---|---|
| | $\beta$ | $\kappa$ | $\theta \times 10^5$ | $\sigma \times 10^{-11}$ | $\omega_{ref} \times 10^4$ | $M_{ref} \times 10^{-3}$ |
| 1 | 1 | | 1.7 | 0.42 | 2.2 | 0.34 |
| | | 0.5 | 0.89 | 0.21 | 1.9 | 0 |
| 2 | 1 | | 0.95 | 1.1 | 3.5 | 0.2 |
| | | 0.45 | 0.39 | 0.51 | 3.5 | 0 |
| 3 | 1 | | 6.3 | 2 | 6.8 | 1.5 |
| | | 0.3 | 1.5 | 0.6 | 6.4 | 0 |
| 4 | 1 | | 5.6 | 3 | 5 | 0.97 |
| | | 0.27 | 1.4 | 1.6 | 5.2 | 0 |
| 5 | 1 | | 3.1 | 1.54 | 3.5 | 1.5 |
| | | 0.27 | 0.53 | 1.2 | 2.6 | 0 |
| 6 | 1 | | 5.8 | 3.4 | 2.7 | 0.88 |
| | | 0.33 | 0.57 | 3 | 1.6 | 0 |

Table 5.2: Output and input variances under conventional and covariance control with feedforward
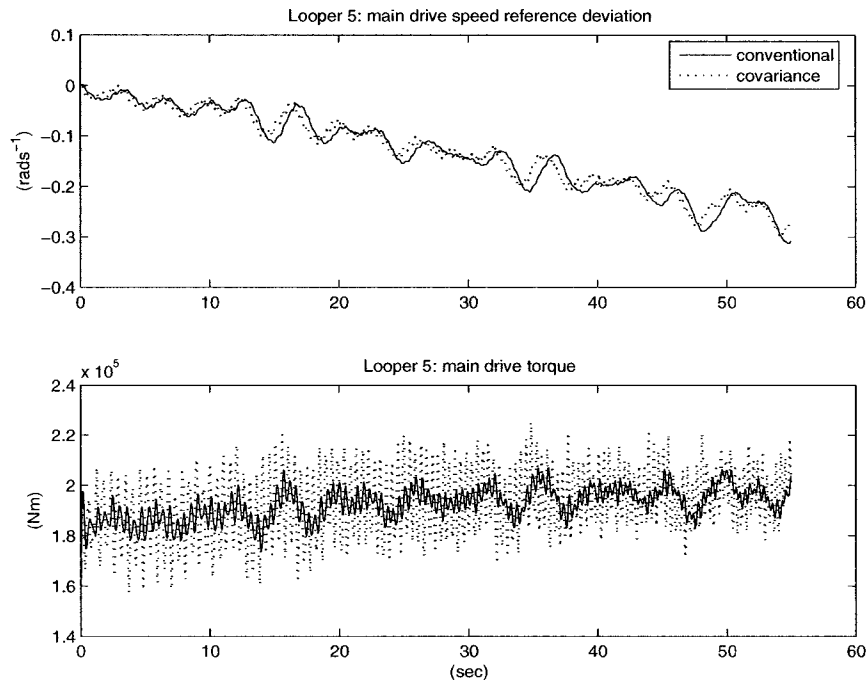


Figure 5.7: Main drive motor torque under conventional and covariance control

Figure 5.7 proves that the input variance may not be a sufficient indicator of the input energy at all times, mainly because it does not contain any information regarding the frequency; it is apparent that although its output variance is smaller, the covariance

controller causes the motor torque vary more because of its high frequency content. This high frequency control at around 2 Hz is due to small roll eccentricity effects but is large in size because of control inefficiency at high frequencies, which has been stated in Section 4.1. It in fact can do little to improve the overall performance and may be prevented if the roll off of the controller at high frequencies is ensured by employing higher measurement noise variances and a high pass noise filter in design.

*"I always avoid prophesying beforehand, because it is much better policy*
*to prophesy after the event has already taken place."*

— Churchill

# 6

# Conclusions

The main conclusions of this study are:

1. In a finishing mill, disturbances are transmitted via two mechanisms:

   i. Strip traveling downstream: Temperature profile is the major disturbance carried downstream by the strip. This profile is not corrected and is influential throughout the mill. Strip gage is not as strong a disturbance because each stand acts like a filter suppressing the gage variations.

   ii. Chain effect: In a finishing mill, the effect of a disturbance introduced at a certain looper travels upstream rather than traveling downstream because each stand's looper controller mainly disturbs the upstream looper. Speed feedforward may significantly reduce this chain effect.

2. The resonance frequency of the looper-strip system is directly proportional to the square root of strip cross sectional area and inversely proportional to the square root of system inertia. Further, for strip of small cross sectional area, the sensitivity to disturbances is larger. Thus, tension control may be difficult for later loopers due to the thin strip with them as well as the higher frequency disturbances they receive from HAGC and faster rotating rolls. It is possible to increase the resonance frequency by

74

some structural changes such as lowering the looper and looper drive inertia. The controlled looper-strip system has an additional sensitivity peak, which is smaller in size and at lower frequencies (less than 1 Hz).

3. Speed feedforward drastically improves control performance. A conventional system using speed feedforward can achieve significantly better performance than a multivariable controller that uses a similar amount of control in absence of feedforward.

4. Covariance control performance can be substantially better than that of conventional control, especially for later loopers. It is important, however, to suppress the controller response at high frequencies where little control can be achieved due to insensitivity to control inputs. It is not realistic to expect efficient control above 1 Hz if control input use is to be reasonable.

5. Covariance control uses a negligible amount of torque whereas conventional control uses large amounts when the looper angle is not regulated well. It can be said that the conventional control's torque use has little dynamic effect and is mainly for removing the offset. In any case, the stand speed appears to be the main input for looper control.

6. Activity of gage controllers has a very strong effect on loopers. Hydraulic pistons manipulated by mill stretch compensators using force feedback may significantly disturb the looper if the force fluctuates due to reasons other than gage variation. This fluctuation could be very small in size (e.g. less than 1% of nominal). Flatness defects might cause such variations.

7. Although the process is very complex and many disturbances are unknown, it is still possible to simulate a finishing mill with reasonable accuracy. It is essential to account for the variable inter-stand transport delay if realistic simulation results are sought. Otherwise a phase shift between the outputs and plant data is inevitable and the effects of the disturbances that accelerate with mill speedup cannot be studied. Most of the dynamics of a finishing mill is at the actuators and detailed modeling of the actuators, especially that of the main drive, also enhances simulation accuracy.

*"The ability to foretell what is going to happen tomorrow, next week, next month and next year. And to have the ability afterwards to explain why it didn't happen."*

— Churchill, explaining the qualities a politician requires

# Future Work

Development of a higher fidelity model and design of higher performance control systems are the two basic areas where the current research work can be expanded.

Despite a number of drawbacks such as unknown disturbances, unknown plant control arrangements and tuning, and the phenomena that are not modeled, the simulation results are promising. Among all these drawbacks, a considerable lack of information about the gage control systems has been the most influential, particularly due to sensitivity of the loopers to the manipulations of the gage controllers. Better simulation of these systems requires better knowledge of the controller structure and tuning and may also require a more detailed stand model. Currently, the finishing mill stand is modeled as a simple spring, whose position changes under roll force variations. If this representation is upgraded to a spring-mass system, it will be possible to account for the stand dynamics and an important step towards accurate simulation of the hydraulic actuators will be taken. It is true that such an improvement will increase the model order but a dynamic stand model may actually decrease the required simulation time because it breaks the algebraic loop in the current model, which is inefficiently handled by many simulation packages.

Many disturbances entering a finishing mill are not measured. Fortunately, most of these are suppressed quickly as the strip travels downstream. On the other hand, the sensitivity of

76

hydraulic gage controllers encourages knowledge of the disturbances reaching them, even if these disturbances are small in size. It has been found that the hydraulic gage control system may significantly disturb the loopers because of flatness defects or gage variations that are presumably small in size. Better knowledge of the finishing mill disturbances such as inlet gage and shape may therefore be very fruitful in enhancing the simulation accuracy. Such knowledge can be obtained by measuring them or studying their effects on mill behavior in greater detail than this study has done. It is noted that to fully investigate the effect of the shape disturbances, a two dimensional model is required, which accounts for the variations across the strip. A two dimensional model, however, may be too computationally costly and laborious to construct. An alternative may be to search the ways to simulate flatness disturbances as force or gage variations that may be equivalent in effect on loopers.

The results of this research as well as of many others and plant implementations indicate that multivariable systems have a clear superiority over the conventional systems in looper control. Among various multivariable control design methods, frequency domain techniques may better suit the designer's needs because the finishing mill disturbances have very specific frequency ranges. In this context, H-infinity control theory may be applied. Incorporation of the gage control system into looper control is another concept that may improve looper control. There may be multiple gage control loops at a stand and it may be difficult or undesirable to include all of these in looper control, but the mill stretch compensation loop may be a good choice due to its strong influence on loopers.

Simple speed feedforward has been investigated in this study and found to drastically improve looper control. It is expected that some improvement is still possible if the full feedforward as described in this thesis can be realized. In order to do this, stand entry and exit gages must be estimated. This estimation task would be too laborious for the small improvement it is likely to introduce in looper control, if it were not for the possibilities it offers in gage control. If a time dependent estimation of entry and exit gages becomes available, this information can be used for gage control in feedforward mode. The estimation task requires precise strip tracking and buffers may have to be used to handle the variable transport delays. This effort may be worthwhile, especially considering that the sensors, which would be used otherwise, are costly and difficult to maintain.

# Bibliography

[1] T.S. Bilkhu, A.F. MacAlister, and P.J. Reeve. Automation and hot strip mill modernization. *IRON STEEL ENG*, 72(8):27–34, 1995.

[2] B. Bulut, M.R. Katebi, and M.J. Grimble. Co-ordinated control of profile and shape in hot strip finishing mills with nonlinear dynamics. *IEE P-CONTR THEOR AP*, 149(5):471–480, 2002.

[3] M.T. Clark and T. Martin. Advanced control for hot strip finishing mill. *Proceedings of the 7. International Conference on Steel Rolling, Chiba, Japan*, 32(3):727–732, 1998.

[4] M.T. Clark, H. Versteeg, and W. Konijn. Development of new high performance loopers for hot strip mills. *IRON STEEL ENG*, 74(6):64–70, 1997.

[5] R. Dhaouadi, K. Kubo, and M. Tobise. Two-degree-of-freedom robust speed controller for high-performance rolling mill drives. *IEEE T IND APPL*, 29(5):919–926, 1993.

[6] T. Eto, T. Fujiwara, A. Yoshida, T. Naoi, T. Mannaka, and Y. Morooka. The automatic tandem and gage control at tandem cold mill. *International Conference on Steel Rolling, Tokyo, Japan*, pages 439–450, 1980.

[7] H. Ford, F. Ellis, and D.R. Bland. Cold rolling with strip tension. *J IRON STEEL I*, 168(5):57–72, 1951.

[8] V.B. Ginzburg. Basic principles of customized computer models for cold and hot strip mills. *IRON STEEL ENG*, 62(9):21–35, 1985.

78

[9] V.B. Ginzburg. *Steel-Rolling Technology*. Marcel Dekker, New York, 1989.

[10] M.J. Grimble and M.R. Katebi. Predictive optimal control of hot strip finishing mills. *IFAC Automation in the Steel Industry, Kyongju, Korea*, pages 15–18, 1997.

[11] R. Guo. Evaluation of dynamic characteristics of hagc system. *IRON STEEL ENG*, 68(7):52–61, 1991.

[12] R. Guo. Analysis of dynamic behaviors of tandem cold mills using generalized dynamic and control equations. *IEEE T IND APPL*, 36(3):842–853, 2000.

[13] S. Gupta and H. Ford. Calculation method for hot rolling of steel sheet and strip. *J IRON STEEL I*, 205(2):186–190, 1967.

[14] G. Hearns and M.J. Grimble. Multivariable control of a hot strip finishing mill. *Proceedings of the American Control Conference, Albuquerque, New Mexico*, pages 3775–3779, 1997.

[15] G. Hearns and M.J. Grimble. Robust multivariable control for hot strip mills. *ISIJ INT*, 40(10):995–1002, 2000.

[16] G. Hearns, P. Reeve, P. Smith, and T. Bilkhu. Hot strip mill multivariable mass flow control. *IEE P-CONTR THEOR AP*, 151(4):386–393, 2004.

[17] H. Imanari, Y. Morimatsu, K. Sekiguchi, H. Ezure, R. Matuoka, A. Tokuda, and H. Otobe. Looper H-infinity control for hot-strip mills. *IEEE T IND APPL*, 33(3):790–796, 1997.

[18] H. Imanari, Y. Seki, K. Sekiguchi, and Y. Anbe. Application of ILQ control theory to steel rolling process. *Proceedings of the 7th International Conference on Steel Rolling, Chiba, Japan, ISIJ*, pages 36–41, 1998.

[19] G. Keintzel, M. Schoisswohl, P. Vorstandlechner, K. Aistleitner, and R. Schneeweis. Advanced control methods in rolling applications. *Proceedings of Industry Applications Conference, IEEE*, 3:2263–2269, 1998.

[20] Y.H. Moon, I.S. Jo, and C.J. Van Tyne. Control scheme using forward slip for a multi-stand hot strip rolling mill. *KSME INT J*, 18(6):972–978, 2004.

[21] T. Oda, N. Satou, and T. Yabuto. Adaptive technology for thickness control of finisher set-up on hot strip mill. *ISIJ INT*, 35(1):42–49, 1995.

[22] M. Okada, K. Murayama, A. Urano, Y. Iwasaki, A. Kawano, and H. Shiomi. Optimal control system for hot strip finishing mill. *CONTROL ENG PRACT*, 6(8):1029–1034, 1998.

[23] D. Partington. Computer control in plate rolling. *International Conference on Steel Rolling, Tokyo, Japan*, pages 205–216, 1980.

[24] M. Pietrzyk and J.G. Lenard. *Thermal-mechanical modeling of the flat rolling process*. Springer-Verlag, Berlin, Heidelberg, 1991.

[25] J.C. Price. The hot strip mill looper system. *IEEE T IND APPL*, (5):556–562, 1973.

[26] G.W. Rigler, H.R. Aberl, W. Staufer, K. Aistleitner, and K.H. Weinberger. Improved rolling mill automation by means of advanced control techniques and dynamic simulation. *IEEE T IND APPL*, 32(3):599–607, 1996.

[27] W.L. Roberts. *Hot Rolling of Steel*. Marcel Dekker, New York, 1983.

[28] Y. Saito, T. Enami, and T. Tanaka. The mathematical model of hot deformation resistance with reference to microstructural changes during rolling in plate mill. *T IRON STEEL I JPN*, 25(11):1146–1155, 1985.

[29] Y. Seki, K. Sekiguchi, Y. Anbe, K. Fukushima, Y. Tsuji, and S. Ueno. Optimal multivariable looper control for hot strip finishing mill. *IEEE T IND APPL*, 27(1):124–130, 1991.

[30] K.N. Shohet and N.A. Townsend. Roll bending methods of crown control in four-high plate mills. *J IRON STEEL I*, 206(11):1088–1098, 1968.

[31] K. Shoji, H. Miura, E. Takeda, and R. Takahashi. Profile and shape control in hot strip mill. *Proceedings of the fourth international conference on steel rolling, IRSID, France*, pages A.21.1–A.21.6, 1997.

[32] R.I. Stephens and A. Randall. On-line adaptive control in the hot rolling of steel. *IEE P-CONTR THEOR AP*, 144(1):15–24, 1997.

[33] R.I. Tessendorf. Mill main drives: Response and mechanical performance. *IRON STEEL ENG*, 69(3):37–41, 1992.

[34] L. Wang and W.R. Cluett. Tuning PID controllers for integrating processes. *IEE P-CONTR THEOR AP*, 144(5):385–392, 1997.

[35] F. Yamada, K. Sekiguchi, M. Tsugeno, Y. Anbe, Y. Andoh, C. Forse, M. Guernier, and T. Coleman. Hot strip mill mathematical models and set-up calculation. *IEEE T IND APPL*, 27(1):131–139, 1991.

[36] L. Zhang and B. Huang. An LMI approach to sub-minimum energy control with output covariance constraints. *Internal Report, University of Alberta*, 2003.

*"I am without an office, without a seat...and without an appendix."*
*– Churchill, struck down by acute appendicitis*

# A

# Calculation of strip inertia

As the looper moves, the parts of the strip designated by $L_L$ and $L_R$ in Figure 2.1 also move, causing the strip angles $\alpha_L$ and $\alpha_R$ to change. These motions are therefore rotations. The inertial load created by rotating the left-hand part on its axis of rotation is:

$$M_L = \int_0^{L_L} (\ddot{\alpha}_L s dm)s = hw\rho\ddot{\alpha}_L \int_0^{L_L} s^2 ds = hw\rho\ddot{\alpha}_L \frac{L_L^3}{3} \tag{A.1}$$

where $s$ is a coordinate along the strip. This torque $M_L$ should be supplied by the looper. Assuming the force at strip-looper contact point is purely vertical and noting that $L_L \approx L_L cos\alpha_L \approx D/2$ for the practical operating range, this can be expressed as:

$$M_L = F_{int}\frac{D}{2} \tag{A.2}$$

Load $M_{int}$ this inertia force $F_{int}$ will create on looper shaft, taking into account that the right-hand part of the strip should have a similar contribution, is:

$$M_{int} = 2F_{int}lcos\theta = \frac{1}{6}hw\rho D^2 l \cos\theta\ddot{\alpha} \tag{A.3}$$

$\alpha$ in Equation A.3 replaces both $\alpha_L$ and $\alpha_R$ which are numerically very similar. A linear relation may be established between the strip angle $\alpha$ and looper angle $\theta$ for the practical working range. This is obvious from Figure A.1. The approximation $\Delta\alpha = \Delta\theta/5$ turns
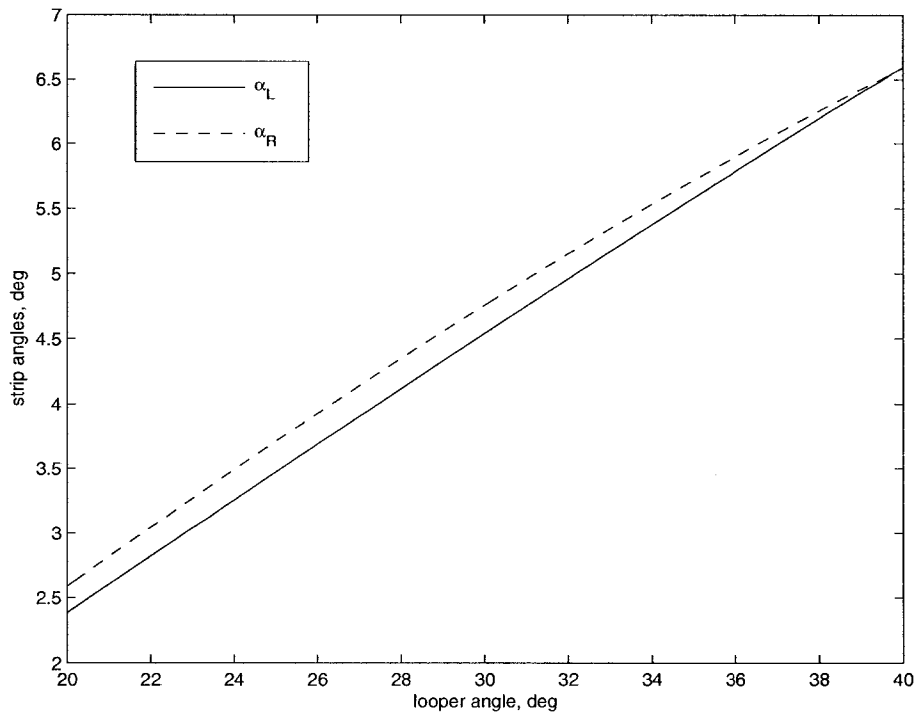
82

Figure A.1: The exact relation between looper and strip angles

Equation A.3 into:

$$M_{int} = \frac{1}{30} D^2 h w \rho l \cos \theta \; \ddot{\theta}$$

(A.4)

from which the strip equivalent inertia $J_s$ on looper shaft can be written as:

$$J_s = \frac{1}{30} D^2 h w \rho l \cos \theta$$

(A.5)

For a strip of cross sectional area 7000 mm², the contribution is:

$$J_s = \frac{1}{30} \times 5.7^2 \times 7000 \times 10^{-6} \times 7500 \times 0.7 \cos 25 = 36 \text{ kgm}^2$$

which is approximately 10% of a low-inertia looper system inertia.

# B

# Calculation of strip bending load

To initiate bending, the bending load $M_y$ should create a stress on strip surface equal to strip tensile yield stress $\sigma_y$. Assuming the neutral plane is halfway through the thickness of the strip, this can be expressed as:

$$M_y = 2\frac{\sigma_y I}{h} \tag{B.1}$$

where $I$ is the second area of moment around the neutral plane and is equal to:

$$I = \frac{1}{12}wh^3 \tag{B.2}$$

The strip may be approximated as a beam with fixed supports at two ends and loaded in the center. According to this, the loads $M_y$ bending force $F_b$ will create at the ends is (Shigley, 1986):
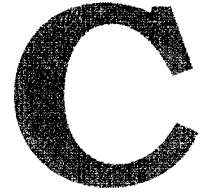
$$M_y = \frac{F_b D}{8} \tag{B.3}$$

Combining the equations, the bending force required at looper-strip contact point can be found as:

$$F_b = \frac{4}{3}\frac{\sigma_y wh^2}{D} \tag{B.4}$$

The load that will be created by this force on looper shaft is:

$$M_b = \frac{4}{3}\frac{\sigma_y wh^2}{D}l\cos\theta \tag{B.5}$$

84

# C

# Summary of model equations

The model equations here are arranged in four sets, each describing a major phenomenon in the finishing mill. Coiler equations are not included.

## C.1 Strip dynamics

$$\dot{\sigma} = \frac{E}{L}\left(\frac{dL}{d\theta}\dot{\theta} - v + V_{i+1}\right)$$

$$L = L_L + L_R$$

$$L_L = [(d + l\cos\theta)^2 + (l\sin\theta + r_l - y)^2]^{1/2}$$

$$L_R = [(D - d - l\cos\theta)^2 + (l\sin\theta + r_l - y)^2]^{1/2}$$

$$v = \omega R_0(1 + f)$$

$$J_{md}G_r\dot{\omega} = M_D - \frac{M_R}{G_r}$$

$$f = \frac{R}{h}\left(\frac{1}{2}\sqrt{\frac{H - h}{R}} - \frac{\sqrt{3}\bar{\sigma}(H - h) + H\Sigma - h\sigma}{4\sqrt{3}\bar{\sigma}R\mu}\right)^2$$

$$V = \frac{vh}{H}$$

85

## C.2 Looper dynamics

$$J\ddot{\theta} = M - M_L - c_f\dot{\theta} - s_f\text{sign}\{\dot{\theta}\}$$

$$M_L = M_\sigma + M_s + M_w + M_b$$

$$M_\sigma = \sigma w\bar{h}[(-\cos\alpha_L + \cos\alpha_R)(l\sin\theta + r_l) + (\sin\alpha_L + \sin\alpha_R)(l\cos\theta)]$$

$$\cos\alpha_L = \frac{d + l\cos\theta}{L_L}$$

$$\cos\alpha_R = \frac{D - d - l\cos\theta}{L_R}$$

$$\sin\alpha_L = \frac{l\sin\theta + r_l - y}{L_L}$$

$$\sin\alpha_R = \frac{l\sin\theta + r_l - y}{L_R}$$

$$M_s = \bar{h}w\rho g(L_L + L_R)l\cos\theta$$

$$M_w = m_L g r_L \cos\theta$$

$$M_b = \frac{4}{3}\frac{\sigma_y w\bar{h}^2}{D}l\cos\theta$$

## C.3 Heat transfer

$$t_i = T_i - \Delta T_c + \Delta T_m$$

$$\Delta T_c = b_1\frac{8k}{\rho c}\frac{(T - T_r)}{H + h}\left(\frac{\sqrt{R_0(H - h)}}{\pi\alpha_r v}\right)^{1/2} \qquad \alpha = \frac{k_r}{\rho c_r}$$

$$\Delta T_m = b_2\frac{K}{\rho c}\ln\frac{H}{h}$$

$$T_{i+1} = \left(b_3\frac{6S\epsilon}{\rho hc}T_i + \frac{1}{(t_i + 273)^3}\right)^{-1/3} - 273°$$

$k_r$ is roll thermal conductivity; $c_r$ is roll specific heat capacity; and $\rho$ is the density of the roll material.

# C.4 Deformation

$$h = C + \frac{F}{K_s}$$

$$R = R_0 \left( 1 + \frac{F}{(H-h)w} \frac{16(1-\nu_r^2)}{\pi E_r} \right)$$

$$F = Kw\sqrt{R(H-h)}$$

$$K = Q\bar{\sigma}$$

$$Q = 0.5(\pi + z_a)$$

$$z_a = \frac{\sqrt{R(H-h)}}{(H+h)/2}$$

$$\bar{\sigma} = \bar{\sigma}^\circ - \frac{1}{\sqrt{3}} \frac{\Sigma + \sigma}{2}$$

$$\bar{\sigma}^\circ = a_1 - a_2 T$$

$$M_R = 2Fa\sqrt{R(H-h)} + (R+h/2)(\Sigma_i \bar{H} - \sigma_i \bar{h})w$$

$$a = 0.594 z_a^{-0.3146}$$

# Calculation of natural frequency

Noting that the nominal speed imbalance $\bar{V}_{i+1} - \bar{v}$ should be zero, the speed imbalance term in Equation 2.21 can be expanded as:

$$V_{i+1} - v = \bar{V}_{i+1} + \Delta V_{i+1} - (\bar{v} + \Delta v) = \Delta V_{i+1} - \Delta \omega R_0(1 + \bar{f}) - \bar{\omega} R_0 \Delta f \qquad (D.1)$$

Among the various factors affecting the slip change $\Delta f$ only forward tension $\sigma$ is a variable of the model considered here. The other contributions can be lumped into a general disturbance term $\Delta V$ together with $\Delta V_{i+1}$ to yield:

$$V_{i+1} - v = \Delta V - \Delta \omega R_0(1 + \bar{f}) - \bar{\omega} R_0 \frac{\partial f}{\partial \sigma} \Delta \sigma \qquad (D.2)$$

Using this expansion and modifying Equation 3.9 as necessary, the following model can be obtained:

$$\dot{x} = Ax + B_u \begin{bmatrix} \omega_{ref} \\ M_{ref} \end{bmatrix} + B_w \Delta V \qquad (D.3)$$

where

$$A = \begin{bmatrix} & 1 & & & \\ -\frac{1}{J}\frac{\partial M_L}{\partial \theta} & -\frac{c_f}{J} & -\frac{1}{J}\frac{\partial M_L}{\partial \sigma} & & \frac{1}{J} \\ 0 & \frac{E}{L}\frac{dL}{d\theta} & -\frac{E\omega R_0}{L}\frac{\partial f}{\partial \sigma} & -\frac{ER_0(1+f)}{L} & \\ & & & -\frac{1}{T_{md}} & \\ & & & & -\frac{1}{T_{cr}} \end{bmatrix}, \quad B_u = \begin{bmatrix} & \\ \frac{1}{T_{md}} & \\ & \frac{1}{T_{cr}} \end{bmatrix},$$

88

$B_w = [\begin{array}{ccccc} 0 & 0 & E/L & 0 & 0 \end{array}]^T$ and $x = [\begin{array}{ccccc} \theta & \omega_L & \sigma & \omega & M \end{array}]^T$. It is remarked that the static looper friction and variation of strip inertia with looper angle are neglected in derivation of Equation D.3.

Looper frequency response to strip speed disturbance $\Delta V$ can be evaluated from Equation D.3 but an analytical expression for looper-strip natural frequency may be tedious to obtain because the system is of third order. A first attempt could be to approximate the system with an extreme case where front tension does not affect the slip at all, i.e. $\partial f/\partial\sigma = 0$, which renders the system third order-integrating. From Equation Set D.3:

$$J\ddot{\theta} = -M_L\{\sigma,\theta\} - c_f\dot{\theta} \tag{D.4}$$

It should be remembered that the inputs other than $\Delta V$ are insignificant for the purpose of this derivation. Taking the Laplace transform:

$$Js^2\Delta\theta(s) = -\frac{\partial M_L}{\partial\sigma}\Delta\sigma(s) - \frac{\partial M_L}{\partial\theta}\Delta\theta(s) - c_fs\Delta\theta(s) \tag{D.5}$$

Keeping in mind the assumption $\partial f/\partial\sigma = 0$, the linear relationship from Equation Set D.3 for tension can similarly be expressed in Laplace domain as:

$$s\Delta\sigma(s) = \frac{E}{L}\left(\frac{dL}{d\theta}s\Delta\theta(s) + \Delta V(s)\right) \tag{D.6}$$

Substituting Equation D.6 into D.5 and regrouping the terms:

$$\Delta\theta(s)\left(Js^2 + c_fs + \frac{\partial M_L}{\partial\sigma}\frac{E}{L}\frac{dL}{d\theta} + \frac{\partial M_L}{\partial\theta}\right) = -\frac{\partial M_L}{\partial\sigma}\frac{E}{L}\frac{\Delta V(s)}{s} \tag{D.7}$$

from which the natural frequency is found as:

$$\omega_n = \left(\frac{1}{J}\frac{\partial M_L}{\partial\sigma}\frac{E}{L}\frac{dL}{d\theta} + \frac{1}{J}\frac{\partial M_L}{\partial\theta}\right)^{1/2} \tag{D.8}$$

The second term in Equation D.8 is negligible in size for all practical purposes.

More insight can be obtained if a simplified, symmetric looper-strip geometry with a strip angle of $\alpha$ is considered. Looper load due to tension in such a case is:

$$M_\sigma = 2\sigma whl\sin\alpha\cos\theta \tag{D.9}$$

Then it follows that:

$$\frac{\partial M_L}{\sigma} = \frac{\partial M_\sigma}{\sigma} = 2whl\sin\alpha\cos\theta \qquad \text{(D.10)}$$

$$\omega_n = \left(2whl\sin\alpha\cos\theta\frac{E}{L}\frac{dL}{d\theta}\frac{1}{J}\right)^{1/2} \qquad \text{(D.11)}$$

If used to estimate the resonance frequency, Equation D.11 gives errors of 6 and 17 % for Loopers 1 and 6 of a typical rolling schedule, which represent the two ends of the parameter range for that rolling schedule.

For modern, low-inertia loopers, mass may be assumed concentrated in the roll and the looper inertia may be approximated as $J \approx m_r l^2$, which changes Equation D.11 to:

$$\omega_n = \sqrt{\frac{whE}{m_r}}\,\varphi \qquad \text{(D.12)}$$

where $\varphi$ is a complex trigonometric function of looper geometric properties. It is remarked here that the two factors of Equation D.12 are completely independent of each other.